An active oblique-contractional belt at the transition between the Southern Apennines and Calabrian Arc: the Amendolara Ridge, Ionian Sea, Italy.

Luigi Ferranti (*, [a]), Pierfrancesco Burrato (**), Fabrizio Pepe (***), Enrico Santoro (*, °), Maria Enrica Mazzella (*, °°), Danilo Morelli (****), Salvatore Passaro (*****), Gianfranco Vannucci (******)

(*) Dipartimento di Scienze della Terra, dell'Ambiente e delle Risorse, Università degli Studi di Napoli Federico II, Napoli, Italy.

(**) Istituto Nazionale di Geofisica e Vulcanologia, Roma, Italy.

(***) Dipartimento di Scienze della Terra e del Mare, Università di Palermo, Italy.

(****) Dipartimento di Scienze Geologiche, Ambientali e Marine, Università di Trieste, Italy

(*****) Istituto per l'Ambiente Marino Costiero, Consiglio Nazionale delle Ricerche, Napoli, Italy

(******) Istituto Nazionale di Geofisica e Vulcanologia, Bologna, Italy.

(°) presently at Robertson, CGG Company, Wales.

(°°) presently at INTGEOMOD, Perugia, Italy.

(a) Corresponding author: L. Ferranti, DiSTAR - Dipartimento di Scienze della Terra, dell'Ambiente e delle Risorse, Università di Napoli "Federico II," Largo S. Marcellino 10, IT-80138 Naples, Italy. (luigi.ferranti@unina.it)

This article has been accepted for publication and undergone full peer review but has not been through the copyediting, typesetting, pagination and proofreading process which may lead to differences between this version and the Version of Record. Please cite this article as doi: 10.1002/2014TC003624

Abstract

High-resolution, single-channel seismic and multibeam bathymetry data collected at the Amendolara Ridge, a key submarine area marking the junction between the Apennines collision belt and the Calabrian subduction forearc, reveal active deformation in a supposedly stable crustal sector. New data, integrated with existing multichannel seismic profiles calibrated with oil-exploratory wells, show that middle to late Pleistocene sediments are deformed in growth folds above blind oblique-reverse faults that bound a regional pop-up. Data analysis indicate that ~10 to 20 km long banks that top the ~80 km long, NW-SE trending ridge are structural culminations above en-echelon fault segments. Numeric modeling of bathymetry and stratigraphic markers suggests that three 45°-dipping upper crustal (2-10 km) fault segments underlie the ridge, with slip rates up to ~0.5 mm/yr. Segments may be capable with M~6.1-6.3 earthquakes, although un unknown fraction of aseismic slip undoubtedly contributes to deformation. The fault array that bounds the southern flank of the ridge (Amendolara Fault System, AFS) parallels a belt of Mw<4.7 strike-slip and thrust earthquakes, which suggest current left-oblique reverse motion on the array. The eastern segment of the array shows apparent morphologic evidence of deformation and might be responsible for Mw≤5.2 historic events. Late Pliocene-Quaternary growth of the oblique contractional belt is related to the combined effects of stalling of Adriatic slab retreat underneath the Apennines and subduction retreat of the Ionian slab underneath Calabria. Deformation localization was controlled by an inherited mechanical interface between the thick Apulian (Adriatic) platform crust and the attenuated Ionian basin crust.

Key points

High-resolution marine geophysics data document active oblique contraction

Blind fault segments underlying shallow-crustal folds are modeled

Reactivation of a passive continental margin drives active tectonics

Index terms:

Marine seismics

Folds and folding

Geomorphological geochronology

Continental margins: convergent

Keywords: seismic reflection profiles, active fault-related folds, blind reverse-oblique fault segments modeling, Ionian Basin, southern Italy

1. Introduction

The characterization of active structures within orogens with low contemporary displacement rates is a difficult task because of the common lack, in the subaerial setting, of a suitable geomorphologic and stratigraphic record of deformation. Within submarine orogenic belts, on the contrary, high-resolution marine geophysical data provide a valuable tool to help deciphering the recent and current deformation pattern [e. g. *Barnes and Nicol*, 2004; *Okamura et al.*, 2005; *Cormier et al.*, 2006; *Nodder et al.*, 2007; *Di Bucci et al.*, 2009; *Polonia et al.*, 2012; *Goldfinger et al.*, 2012].

These difficulties and opportunities are typified in the area of southern Italy, where rapid Neogene north-easterly migration of the Apennines collision belt toward the Adriatic-Apulian foreland and southeastward emplacement of the Calabria forearc sliver toward the Ionian basin [Figures 1a, 1b; *Patacca et al.*, 1990; *Faccenna et al.*, 2001; *Polonia et al.*, 2011] contrasts with the modern deformation characterized by dominant hinterland extension and quiescent frontal thrust belt activity [*Pondrelli et al.*, 2006; *D'Agostino et al.*, 2011].

The seaward continuation of the Apennines belt in the Taranto Gulf, a major embayment of the Ionian Sea, is represented by the >80 km long Amendolara Ridge (Figure 1a). Although workers have suggested that the ridge has grown as a result of Pliocene-Quaternary transpressional or oblique-reverse displacement [*Del Ben et al.*, 2007; *Ferranti et al.*, 2009], detailed images of the recent tectonic activity are lacking.

The oceanographic cruise Teatioca_2011 was purportedly devoted to acquire high-resolution geophysical data on the Amendolara Ridge in order to demonstrate the occurrence and mode of recent tectonics. Results of the cruise support the hypothesis that deformation is occurring today beneath the ridge and is accommodated by growth of fault-propagation folds above oblique thrust ramps. The high-quality datasets allow investigation how relatively small but detectable deformation is accommodated by the several segments composing the system. When integrated with existing multi-channel seismic (MCS) profiles, deep borehole logs and seismicity data, the new dataset allows the compilation of a feasible model of active crustal deformation in the regional tectonic context.

Documentation of active deformation beneath the Amendolara Ridge carries important seismotectonic implications. This part of southern Italy is characterized by a low level of historic and instrumental seismicity when compared to the hinterland extensional province, and is considered tectonically stable by most researchers [e. g. *Pondrelli et al.*, 2006; *D'Agostino et al.*, 2011, *Pierdominici and Heidbach*, 2012; *Presti et al.*, 2013]. Indeed, the region suffered from moderate but locally damaging earthquakes caused by debated or

unknown sources [*DISS Working Group*, 2010]. Characterization of the proper geometric and segmentation model for the Amendolara Ridge is thus vital to better assess the seismic hazard of this populated coastal area of southern Italy.

Detailed characterization of the crustal deformation pattern at the Amendolara Ridge also provides quantitative information to construct models of regional tectonism. We show that Quaternary oblique contraction occurs behind the frontal thrust of the Apennines and hints at a complex interaction between the Apennines and Calabrian Arc. Rapid Miocene-Pliocene north-east motion of the Apennines thrust belt evolved during eastward roll-back of the Adriatic slab [*Malinverno and Ryan*, 1986; *Patacca et al.*, 1990]. By the early Pleistocene, stalling of slab roll-back beneath the Apennines is testified by the cessation of frontal thrust displacement [*Hippolyte et al.*, 1994; *Patacca and Scandone*, 2007]. During Pliocene-Quaternary, however, displacement of the Calabria subduction forearc still occurred [*Polonia et al.*, 2011].

The study area lies at the transition between the Apennines and Calabria and has the potential to preserve the record of the complex interaction between the two segments of the central Mediterranean orogen. Development of the Amendolara Ridge during late stages of Apennines tectonism may hint at an oblique convergence between different crustal blocks underlying the Ionian and Adriatic seas (Figure 1b). Overall, results reported here highlight the role of inherited crustal weaknesses in driving localization of deformation.

2. Regional tectonic setting.

The Amendolara Ridge floors the southern Taranto Gulf at the transition between the Southern Apennines and Calabrian Arc segments of the central Mediterranean orogen (Figures 1a, 1b). Growth of the Apennines and Calabrian belts occurred during Neogene west-directed subduction and east-directed roll-back of Adria, a lithospheric block or micro-plate formerly connected to north Africa that drifted away from it during the Mesozoic [*Malinverno and Ryan*, 1986; *Gueguen et al.*, 1998; *Faccenna et al.*, 2001; *Catalano et al.*, 2001]. The Adria plate is composed of two dissimilar crustal sectors, as reflectd in the bathymetry (Figure 1b). Whereas the shallow Adriatic Sea region to the northeast is floored by continental crust, the deep Ionian Sea to the southwest is thought to lay upon thinned continental or oceanic crust related to stretching and rifting [*De Voodg et al., 1992; Catalano et al.*, 2001]. The margin between the two crusts lies beneath the Ionian Sea and projects to the northwest in Calabria, underneath the accretionary wedge (Figures 1a and 1b). The paired margin between Ionian crust and African continental crust is located on the Sicily eastern

slope (Figure 1b).

The southern part of the Adriatic continental block, which crops out in the Apulia region of southern Italy, is rimmed to the east by the west-verging Dinarides, Albanides and Hellenides, and to the west by the east-verging Apennines (Figure 1b). The Adriatic sector served as a foreland for both fold and thrust belts during their Neogene emplacement [*Roure et al.*, 1991; *Menardi-Noguera and Rea*, 2000; *Nicolai and Gambini*, 2007]. Conversely, the stretched and rifted Ionian block represents the foreland for south-directed motion of the Calabrian forearc terrane and of its frontal accretionary wedge [*Malinverno and Ryan*, 1986*; Pepe et al.*, 2010; *Polonia et al*., 2011].

Rapid roll-back of the Ionian and southern Adriatic sectors of Adria, and related orogenic migration are thought to have occurred during Miocene-Pliocene, but during the Quaternary, displacement rates slowed substantially both in the Apennines and in Calabria [*Faccenna et al.*, 2001]. Today, only limited subduction of the seismically active part of the Ionian slab beneath Calabria (Figure 1b) is suspected [*D'Agostino et al.*, 2011], with active shortening taken up by outward motion of the accretionary wedge in the deep Ionian Sea [*Polonia et al.*, 2011]. In the Southern Apennines, motion of the frontal thrust belt ceased during early Pleistocene as the front was buried beneath the western margin of the Bradano foredeep basin [Figure 1a; *Patacca and Scandone*, 2007]. Offshore, motion of the Apennnies thrust front submerged beneath the Taranto Gulf (Figure 1a) is suspected but poorly defined [*Butler*, 2009; *Volpi et al.*, 2011]. To the east, the fronts of the Dinarides, Albanides and Hellenides are seismologically and geodetically active [*Jouanne et al.*, 2011].

In the western or hinterland sector of the Apennines and Calabria, Pliocene demise of contraction was replaced by extensional faulting related to stretching in the Tyrrhenian back-arc basin [Figures 1a, 1b; *Patacca et al.*, 1990*; Hippolyte et al.*, 1994; *Monaco et al.*, 1998; *Spina et al.*, 2009] and to uplift of the mountain belt [*Westaway*, 1993; *Ferranti and Oldow*, 2005]. An array of normal faults is traced along the axis of the chain (Figures 1a, 2), and shows geologic, seismologic and geodetic evidence of activity [*Papanikolaou and Roberts*, 2007; *Ferranti et al.*, 2014].

Since middle Pleistocene, the coastal sector of the Apennines abutting the Ionian Sea has experienced vigorous uplift (~1 mm/a and locally more) [*Westaway*, 1993; *Cucci and Cinti*, 1998; *Ferranti et al.*, 2009; *Santoro et al.*, 2009; 2013; *Caputo et al.*, 2010]. Uplift is manifested by staircases of raised paleo-shorelines, whose deformed profiles embeds both a long- and a short-wavelength component. Whereas the long-wavelength component is attributed to deep-sourced, regional uplift of southern Italy, the short-wavelength component

is argued to reflect local folding and faulting [*Ferranti et al.*, 2009; *Caputo et al.*, 2010; *Santoro et al.*, 2013].

Based on morphotectonic and structural data, *Ferranti et al.* [2009] contended that middle-late Pleistocene terrace folding along the flanks of the Pollino and Valsinni ranges west of the Amendolara Ridge (Figure 2) was caused by motion on underlying blind transpressional faults. The traces of southwest-directed oblique-reverse faults are located at the southern front of the Pollino mountain range [*Monaco et al.*, 1998; *Ferranti et al.*, 2009]. On the opposite northeast-directed blind thrusts bound to the north the Valsinni Ridge (Figure 2), which grew during the early Pleistocene [*Hippolyte et al.*, 1994; *Patacca and Scandone*, 2007]. Fault numerical modeling of the deformed marine terraces [*Santoro et al.*, 2013] suggests active uplift of two opposite-dipping fault-propagation folds linked to blind oblique-thrust ramps located underneath the coastal ranges (Figure 2).

3. Structural framework of the Taranto Gulf.

The Taranto Gulf can be divided into three main morpho-structural sectors. The north-eastern sector has a well-developed shelf, with a smooth morphology representative of the foreland area (Figures 1a, 1c). It is floored by the western part of the Apulian Swell, which is an NW-SE elongated ridge culminating with the Apulian peninsula (Figure 1c). The swell is made of an ~6 km thick Mesozoic-Cenozoic carbonate platform succession resting on an ~35 km thick crust [*Aroux et al.*, 1999; *Doglioni et al.*, 1999].

The central sector has a very narrow shelf incised by a deep trough (the Taranto Valley; Figures 1a, 1c, 2), which is located at the foot of the frontal thrust belt and hosts the submerged part of the Apenninic foredeep basin [*Senatore et al.*, 1988].

The southwestern sector is also floored by a narrow shelf and by the slope to the Ionian Sea. This sector is characterized by ridges and intervening basins (Figures 1c, 2) that are the morphologic expression of imbricates and folds of the Apennines thrust belt [*Butler*, 2009; *Volpi et al.*, 2011]. The Apulian carbonate platform, lying to the northeast in the Apulian Swell, plunges to the southwest underneath the submerged foredeep basin and the thrust belt (Figure 1c). The Apulian carbonates can be traced west until beneath the Amendolara Ridge, and are lost farther west under the northern Calabria coast. High-penetration seismic reflection profiles coupled with oil-exploratory wells show that the Apulian platform rocks are involved in thrusting beneath the frontal belt of the Apennines both on-land and offshore [*Menardi-Noguera and Rea*, 2000; *Nicolai and Gambini*, 2007; *Ferranti et al.*, 2009; *Butler*, 2009], where they form structural highs and lows (Figure 2).

Bathymetric data and seismic reflection profiles in the southern Taranto Gulf demonstrate the offshore continuation of the structures mapped on-land. The seaward projection of the Pollino and Valsinni structural highs coincides with the Amendolara Ridge (Figure 2). Offshore the Sibari Plain, the Sibari-Corigliano Basin is filled locally by >2.5 km of Pliocene-Quaternary deposits and parallels the steep southern scarp of the Amendolara Ridge (Figure 2). Seismic reflection profiles across the Sibari Basin and Amendolara Ridge suggest that the Miocene-Pliocene thrust belt is offset by deeper faults which cut across the underlying Apulia unit [*Del Ben et al.*, 2007; *Ferranti et al.*, 2009]. Farther offshore, a regional seismic profile located ~100 km southeast of the Amendolara Ridge shows, on the seaward projection of the ridge, a backthrust belt rooted at or beneath ~5 sec (~7 km depth) [Figure 1c; *Doglioni et al.*, 1999].

4. Materials and Methods.

Swath bathymetric mapping of the sea-floor, a grid of high-resolution (Geo-Source Sparker) and very high-resolution (Sub-bottom Chirp) single-channel seismic (SCS) reflection profiles (Figure 4a), and shallow coring were carried on during January 2011 (Teatioca_2011 cruise) onboard the oceanographic vessel Urania of the National Research Council (CNR). Positioning was controlled by Differential Global Positioning System.

The echo-metric data processing was performed by using the PDS2000 software (Reson), which provided a Digital Terrain Model (DTM) with a spatial resolution range between 2 and 10 m (Figure 4). Multibeam data covered an area of approximately 1100 km^2 including the continental shelf and slope of the Amendolara Ridge and part of the adjoining basins to a depth of ~1000 m.

The Sub-Bottom Chirp profiler operated with a 16 transducer Benthos Chirp II system in a wide frequency band (2–7 kHz), with a long pulse (20–30 ms). Signal penetration was exceeding 125 ms, two-way time (TWT) in the deeper sector of the study area.

The acoustic source used to acquire the high-resolution seismic data was a 1 kJ Sparker power supply with a multi-tips Sparker array, which lacks ringing and has a base frequency around 800 Hz, fired at 1.5s time interval. Data were recorded with a single-channel streamer having an active section of 2.8 m and containing seven high-resolution hydrophones, for 1.3 s two way time (t.w.t) at 10000 Hz (0.1 ms) sampling rate.

Data processing was performed using the Geo-Suite software package running the following mathematical operators: true amplitude recovery using a T2 spherical divergence correction; band-pass (300-2000 Hz) “finite impulse response" filter using a filter length of

256 samples, swell-filter to compensate for sea swelling, mixing of three traces for enhancing horizontal signal, time variant gain to boost amplitudes of deeper arrivals and mutes to eliminate the signal noise on the water column. Signal penetration was found to exceed 500 ms t.w.t.. The vertical resolution is up to 0.5 m near the seafloor.

Following the seismic facies analysis, the SCS lines were depth-converted using velocity intervals of 1500, 1700 and 1800 m/s for the water column, upper Pleistocene-Holocene and lower-mid Pleistocene sedimentary units, respectively. Correlation between seismic units, stratigraphy, and seismic velocities is based on seismic facies analysis and available stratigraphic data areas as illustrated in the Result section.

High-penetration MCS reflection profiles (acquired for oil exploration and available in printed PDF data format only, together with exploratory well logs, through the project VIDEPI: http://unmig.sviluppoeconomico.gov.it/videpi/), which partly overlap with the new SCS profiles grid (Figures 3a, 7), offered constraints on the upper crustal geometry of the ridge and adjacent basins. The MCS profiles were shot in 1975 by the Compagnie Generale de Geophysique (CGG), Massy, France. A Vaporchoc (depth 6 m) and a 48-channel streamer (depth 19 m), with 50 m group interval, were the hardware components used during seismic prospecting. Shot interval was 25 m, resulting in 48-fold coverage. Seismic signals were recorded for 6.0 s TWT at 4 ms sample rate. The multichannel seismic data processing was carried out by the CGG in 1975 by applying the following mathematical operators: amplitude recovery, stabilization by vaporchoc signal, muting, deconvolution, velocity analysis, normal move out and stack of the CDP, time variant filters and trace equalization.

For our research work, we have converted the images of seismic profiles in SGY seismic data format using the GeoSuite AllWorks software, which is a comprehensive GIS environment for processing and interpretation of geological/geophysical data. We interpreted the MCS profiles based on seismic facies analysis calibrated using the deep well logs. Sonic logs, available for some wells, have been used to constrain the seismic velocity for each seismic unit and used for the time to depth conversion of seismic profiles.

Tectonic and stratigraphic information derived from new and existing marine geophysical data were then blended to build a numerical model of active faults underlying the Amendolara Ridge. The parameterization derives from standard dislocation modeling of slip on buried, rectangular-shaped faults embedded in an elastic half-space, and are based on the theoretical formulation of *Okada* [1985]. Such modeling reproduces the surface deformation induced by slip at depth during an earthquake, and is calibrated against the shape of deformed horizons (i.e. bathymetry and subsurface geology as derived from the interpretation of

Multibeam data and of SCS and MCS profiles, respectively), on the assumption that shape arises from the long-term activity of the underlying fault. The best-fitting fault location and geometry (length, width, angle of dip, minimum and maximum depth) were constrained based on iterative comparison between the observed shape of deformed markers and the predicted displacement output of models. The numeric models were performed using the Fault Studio software (a technical report of the version 1.1 is provided by *Basili, R.*, INGV, http://www.earth-prints.org/handle/2122/1039), a MapBasic application which uses a geographical interface. In the final step, fault dislocation modeling was used to calculate the fault slip rates.

Finally, the seismicity pattern of the study region and surroundings was obtained by merging some seismic catalogues that cover different time spans: the Parametric Catalog of Italian Earthquakes (CPTI11, *Rovida et al.* [2011]) with earthquakes from 1005 to 1981; the International Seismological Centre (ISC, *ISC Bulletin* [2011]) with earthquakes from 1904 to 1981; the Italian catalog with homogeneous Mw (GASP, *Gasperini et al.* [2013]) with earthquakes from 1981 to present. For the overlapping period from 1904 to 1981, when a same earthquake is available in CPTI and ISC, we prefer the CPTI event, which generally performs a more robust analysis for location and magnitude using local and global data (see *CPTI Working Group*, [2004]). Both GASP and ISC catalogs provide re-evaluated proxy Mw [*Gasperini et al., 2013a,b; Lolli et al.*, in press]. Focal mechanisms provide a framework of the coseismic strain by event available (table S1) from different datasets: Global Centroid Moment Tensor (GCMT, [*Dziewonski et al.*, 1981]), European-Mediterranean Regional Centroid Moment Tensor (RCMT, *Pondrelli et al.* [2002, 2006, 2011]), Time Domain Moment Tensor (TDMT, *Scognamiglio et al.* [2009]), and Earthquake Mechanisms of Mediterranean Area (EMMA, *Vannucci and Gasperini* [2003, 2004, 2010]). For TDMT catalog a Mw correction according to *Gasperini et al.* [2012] is applied. When a solution is available in more than one catalog, we selected a preferred solution by using criteria as in *Vannucci and Gasperini* [2003].

5. Results

5.1. Morphotectonics of the Amendolara Ridge.

The new multibeam mapping of the sea-floor illustrates with fine detail the salient morphostructural features of the Amendolara Ridge. The ridge is ~80 km long and ~20 km wide, and stretches from the continental shelf to the lower slope of the southern Taranto Gulf

(Figure 3a). The shelf at and around the ridge is very narrow (maximum distance from coast: 7 km), locally absent due to retrogressive canyon erosion. Generally, the slope is characterized by an irregular morphology incised by deep gullies, that extends beneath water depths of 150–200 m (Figure 3a).

The Amendolara Ridge joins the Calabria coast to the west at the Roseto Capo Spulico Head and deepens to the southeast. Standing above this regional slope, four different seamounts or banks are encountered whose minimum depth accordingly deepens to the southeast (Figure 3a). The western and shallower Amendolara Bank, topping at -24 m below sea level (b.s.l.), stretches for ~18 km from a submarine saddle ~10 km off the coast to a steep southeast-facing escarpment down to -350 m b.s.l. From the base of the escarpment, the ridge bifurcates into two parallel branches. The main or southern branch culminates with two distinct banks. The western, Rossano Bank (top at -175 m b.s.l.) stretches for ~15 km and features two minor ridges to the north and northeast. A saddle at ~300 m separates the Rossano from the ~18 km long Cariati Bank (top at - 232 m b.s.l.) to the southeast. A ~12 km long, 5 km wide, northeast-trending furrow (Corigliano Channel) at 800-900 m b.s.l. limits the Cariati Bank from the ~18 km long, deeper Cirò Bank (not investigated in this study) further southeast. The northern ridge, which branches east from the Amendolara Bank, is separated from the southern ridges by a 30 km long, 5 km wide channel, here named Amendolara Channel, whose bottom is steeper and irregular at the head, but becomes flat downslope. The ~30 km long northern ridge (here named Capo Spulico Ridge, topping at -350 m b.s.l.) displays a sharp crest with several hog-back-type culminations.

All these ridges have a remarkably consistent asymmetric profile, with steep southwestern flank and gently sloping northeastern flank. The maximum height of the southwestern scarp increases eastward from ~350 m, ~400 m, ~500 m in the Amendolara, Rossano, and Cariati banks, respectively. The maximum height of the Capo Spulico scarp is ~350 m.

The Amendolara Ridge is bounded to the southwest and northeast by the Sibari-Corigliano and Amendolara Basins, respectively (Figure 3a). At a water depth of ~200–800 m, the <20 km wide Sibari-Corigliano Basin is nestled between the northeastern Calabria continental slope and the Amendolara Ridge. The basin is divided in two depocenters. The shallower western part (Sibari Basin) lays flat in front of the Amendolara Bank, and is separated by a broad saddle from the eastern section (Corigliano Basin), which is narrower and faces the Rossano Bank. Unlike the Sibari-Corigliano basin, which is narrow and elongated, the Amendolara basin to the north is broadly equilateral (Figures 2, 3a).

5.2. Seismo-stratigraphic architecture of Upper Quaternary deposits.

5.2.1. Seismic Units

A number of stacked seismic units, which are bounded by unconformities or para-conformities, have been identified within the SCS profiles in the first 200-300 m below the sea-floor (Figures 4a to 4f). Seismic units are characterized by a rhythmic alternation of seaward-dipping, high-amplitude and laterally continuous reflections, and of low-amplitude reflections. The shallowest sequence S1 is limited at the bottom by U1, which unconformably cuts the underlying sequences on the shelf and progressively becomes a paraconformity on the slope (Figures 4a to 4f, 5a to 5c).

On the shelf, nine seismic units (S1 to S9; Table 1) have been recognized, which are limited by a landward-converging wedge of bounding surfaces (Figures 4a, 4c, 4d). The thickness of seismic units, although dissimilar and variant in profiles from different parts of the ridge, is broadly constant on the shelf and is typically ~30-40 m (Figure 5a, 5b).

5.2.2. Age attribution

The most recent unit, S1, is assigned to the latest Pleistocene-Holocene age because it overlays the widespread surface (U1) carved during the sea-level lowstand of the Last Glacial Maximum (LGM), aged at ~20 ka [*Lambeck et al.*, 2011].

In light of the lack of quantitative age information, the underlying seismic units are broadly bracketed in age by using constraints from on-land outcrops and offshore boreholes. The Lucia well, located straightly upon profiles Tea_10 and Tea_36 (Figures 3a, 4a, 4b), records a transition from unrecovered material, which in the Ionian shelf is generally middle-upper Pleistocene sandy to silty mud, to the lower Pleistocene Subapennine Clay, a readily distinguishable package of compacted clay with regional distribution [*Patacca and Scandone*, 2007]. The depth of this stratigraphic transition in the well nearly coincides with the base of the mapped unconformities (Figures 4a, 4b).

Correlation between the offshore wells and coastal exposures of the Subapennine Clay (Figure 3a) supports this attribution. Along the Pollino coast, the topmost layers of the clay dips 6°-14° seaward, and nannoplancton analysis revealed an uppermost early Pleistocene age [*Di Donato*, pers. comm.]. The top of the same clay has similar recorded dip values in wells, where it forms the base of the middle-upper Pleistocene regressive sequences (Figure 3a).

Based on the above arguments, the stacked seismic units imaged by the SCS profiles are attributed to the middle Pleistocene-Holocene interval (the last ~800 ka; Table 1). The observation that the seismic units on the shelf have broadly comparable thickness and similar

reflector internal geometry supports the notion that each of them formed during the time interval of comparable duration (~100 ka) that characterizes the middle Pleistocene-Holocene eustatic cycles [*Waelbroeck et al.*, 2002; *Lisiecki and Raymo*, 2005]. These packages represent the distal, finer sedimentary counterpart, of the coarse, terraced coastal deposits that are uplifted along the flank of the Pollino Range [*Santoro et al.*, 2009].

The stratigraphic architecture of middle-late Pleistocene sequences indicates uplift during deposition. This is documented by the observation that, except for S1, only the sedimentary record of the falling and lowstand systems tracts are preserved ("forced-regression sequences"). This pattern is typically observed in sectors of the central Mediterranean shelf affected by uplift [*Ridente and Trincardi*, 2002; *Pepe et al.*, 2003; 2013].

5.3. Shallow structural geometry of the Amendolara Ridge from SCS data.

Three-dimensional analysis of the Sparker profiles reveal that the Pleistocene deposits are deformed into broad-wavelength folds, which define a kinematically linked structural system (Figure 3b). Individual folds can be recognized beneath the banks, which culminate the ridge, and partly beneath the shelf to the northwest. The structures are described below, moving from shallower to deeper water depths.

5.3.1. The shelf.

Two northwest-trending anticlines are traced east of Roseto Capo Spulico with wavelength of 5-6 km (Figure 3b). Due to the landward limit of the survey, the folds can be traced for a minimum length of 7-8 km, but they probably extend farther northwest and are connected to the folds exposed on land in the Valsinni Ridge. The western fold appears broader and more open, and the eastern fold is narrower (fold hinges at shot points ~3000 and ~5300, respectively, Figure 4b). A weak northeast fold asymmetry is observed for both folds, consistent with the vergence documented for the Valsinni anticline on-land [*Hippolyte et al.*, 1994], and with the modeling of uplifted coastal terraces [*Santoro et al.*, 2013].

A southern, broad fold is detected in the southern part of the shelf west of the Amendolara Bank (Larissa fold, Figures 3b, 4b). This structure does not have a bathymetric expression, but its deeper crustal expression has been drilled by the Larissa well (Figure 3a). The structure likely connects on-land to the major anticlinorium represented by the Pollino Range.

5.3.2. Amendolara Bank.

The anticline underlying the Amendolara Bank (Amendolara fold) is shifted ~5 km south from the eastward termination of the Valsinni folds, and has a west-northwest-trending

axial trace that is rotated ~40° west relative to the latter folds (Figure 3b). To the west, the western part of the Amendolara fold is almost along-strike with the Larissa fold (Fig. 3b), but bathymetry data suggests the two are not linked. Unlike the Valsinni and Larissa folds, which are buried under the shelf due to a high sediment supply, the morphology of the Amendolara Bank directly reflects the major anticline (Figures 4c and 4d) that can be traced parallel to the long axis of the bank (Figure 3b). The shape of the Amendolara fold changes from cylindrical in the west (Figure 4c) to box in the east (Figure 4d).

Overall, the fold shows beds steepening progressively toward the Sibari basin. A main break in slope at ~200-250 m b.s.l. marks the location where the reflector dip within the middle-upper Pleistocene panel became steeper (around shot point 2500, Figure 4c), and a further increase in dip is observed at the base of the submarine scarp which limits the southern side of the bank at ~350-400 m b.s.l. (shot points 3000 and 1500 in Figures 4c and 4d, respectively). Kinks with locally over-steepened beds are also observed on the northern side of the anticline toward the Amendolara Basin (shot point ~3750, Figure4).

Very high-resolution Chirp profiles document that U1 is also involved in broad folds (Figure 5a), which are parasitic to the main bank-flooring structure, and is locally offset by drag faults related to folding (Figure 5b).

5.3.3. Rossano Bank.

The transition between the Amendolara and Rossano folds occurs at a marked southeast-facing submarine scarp, which limits eastward the Amendolara Bank (Figure 3b). The trend of the ~12 km long Rossano fold is northwest and diverges of ~30° eastward from that of the Amendolara fold. A minor-length (~5 km) monocline fold is found north of the eastern part of the Rossano fold (Figure 3b).

In detail, the Rossano fold forms a fold train with gentle southwestern asymmetry (Figure 4e). On the south-western side of the bank, two >100 m scarps are formed by the steeply rotated beds (shot points ~6000 and ~6750, respectively, Figure 4e).

5.3.4. Cariati Bank and Capo Spulico Ridge.

The Cariati Bank is shifted to the north relative to the Rossano Bank, and is underlain by two west-northwest trending, right-overlapping folds with a cumulative length approaching 20 km (Figure 3b). Unlike the Amendolara fold, the morphology of the Rossano folds is markedly asymmetric, with a crest found at the southwest rim of the bank, and an overall northeast-tilt (Figure 4f). In front of the main fold, a train of minor folds faces the Corigliano basin. The trailing fold is limited by a ~50 m scarp at the sea-floor (outer scarp,

Figure 4f), whose detailed image is provided by the Chirp profile (Figure 5c). Beneath the scarp and within the high-standing block, seismic reflections are disturbed and opaque, suggesting exposure of older rocks due to fault offset, consistent with the rectilinear pattern of the scarp in map view (Figure 5a). The footwall block of this fault on the slope in front of the main bank forms a folds train (Figure 4f) which, as chirp profiles reveal (Figure 5c), involve the sea-floor and the LGM paraconformity. Although the nature of the fault is not clarified by available data, we suggest a NE-dipping reverse component to be consistent with structures exposed in the footwall.

A taller (~220 m), inner scarp (shot points ~1700 to 1900, Figure 4f) separates the frontal folds train from the main fold flooring the bank. At the foot of this inner scarp, reflections ~200 m beneath the sea-floor appear disturbed, suggesting drag along a deep fault that, based on the overall fold asymmetry, is interpreted to dip northward beneath the bank (Figure 4f). The main bank-flooring folds have a wavelength of ~8 km, and are characterized by parasitic folds and faults (between shot points ~2000-2500).

The Cariati Bank is separated from the Capo Spulico Ridge to the north by the Amendolara Channel. Although a lateral correlation of seismic reflections between the two morphological highs across the channel is prevented by diffuse slumping on the slopes, simple projection of reflectors indicates structural uplift of the Capo Spulico Ridge relative to the Cariati Bank (Figure 4f). It is not possible to document whether uplift is accommodated by a fault at the base of Capo Spulico Ridge, or by folding.

5.3.5. Lateral variability in fold geometry.

To establish the lateral extent of individual folds along the Amendolara Ridge, we constructed profiles of fold amplitudes parallel to the ridge elongation (Figure 6; see trace in Figure 3b). This was accomplished by measuring the fold amplitude for horizon U5 in each across-ridge profile, between the hinge of the anticline in the bank and the hinge of the syncline in the Sibari and Corigliano basins [e.g. *Nicol et al.*, 2002; *Di Bucci et al.*, 2009]. The spacing of Sparker profiles used to constrain the amplitude profile of folds is reasonably tight (2-3 km and locally 5-6 km, Figures 3a, 6), and thus the deformation pattern appears well determined. We choose U5 because it tops a transparent seismic unit with occasional low-amplitude reflections, and thus it can be identified and traced from the ridge to the basins with a plausibly good degree of confidence.

All folds have bell-shaped longitudinal profiles suggesting the existence underneath of laterally defined fault segments. Based on this assumption, the lateral change in fold amplitude allows to estimate the corresponding variation in deformation accommodated on

individual fault segments, and to search for the position of segment boundaries.

In detail, the longitudinal profile of fold amplitude shows the sharp termination of the Valsinni fold and the overlapping growth of the Amendolara fold (Figure 6). The Amendolara fold can be confidently traced for ~12 km, but the amplitude shape suggests that it can stretch up to ~20 km. The Cariati fold to the southeast has an amplitude longitudinal profile similar in shape, length and magnitude to the Amendolara fold (Figure 6). We must note that because of deeper water depth and lesser quality of data, substantial uncertainty exists on the estimation of U5 position beneath the basin south of the Cariati bank. However, such limitation does not impact the reconstructed fold longitudinal shape.

The amplitude of the Rossano fold is nearly half that of the adjacent Amendolara and Cariati folds, and the estimated length does not exceed ~15 km (including the contribution of the minor fold to the north of the main fold). Similar geometric features characterize the Capo Spulico Ridge fold. When the individual amplitude of the Rossano and Capo Spulico folds are combined, however, the aggregate throw measured on U5 across the Rossano and Cariati banks (cumulative profile in Figure 6) is almost constant. The geometric pattern, with distributed folding at the Rossano Bank and Capo Spulico Ridge, supports the contention that only two fault segments exist underneath the Amendolara and Cariati banks, and thus of an interposed segment boundary at the Rossano Bank (Figure 6).

5.4. Deep structural geometry of the Amendolara Ridge from MCS data.

5.4.1. Seismo-stratigraphic and structural architecture

Reflectors imaged by MCS profiles, once calibrated by drillings (Figures 8, 9), represent excellent markers that can be laterally traced and bound regionally correlated [e.g. *Minelli and Faccenna*, 2010; *Spina et al.*, 2011; *Capozzi et al.*, 2012] depositional packages. The uppermost unit is characterized by sub-parallel high-frequency and low-amplitude reflections, and corresponds to the Pliocene-Quaternary deposits (Figures 8, 9). The thickness of the unit increases moving offshore from the Sila shelf to the Sibari-Corigliano Basin to ~2.5 km and locally over, and decreases again on the Amendolara Ridge and Pollino shelf (Figures 7, 8). Within this unit, the abrupt transition between middle-upper Pleistocene sand and silty clay, and the underlying upper Pliocene-Pleistocene clay is seismically characterized by a high-amplitude and continuous reflector (Figure 9a), and locally allows distinction of two sub-units.

The base of the Pliocene-Quaternary sequence is marked by a relatively continuous and high-amplitude reflector (Figure 9). This reflector corresponds to a horizon of regional

significance (M- or A-reflector) associated with the top of evaporites and clastic sediments deposited during the late Messinian salinity crisis, or with an erosional unconformity formed during the late Messinian sea level fall [*Ryan*, 1969; *Finetti and Morelli*, 1973; *Malinverno et al.*, 1981].

Underneath the Sila shelf and Sibari-Coriglino basin, horizon M overlies a faintly reflective sequence characterized by poorly continuous reflections, attributed to Upper Messinian continental or transitional clastics [Figure 10a; *Cita and McKenzie*, 1986; *Cavazza and DeCelles*, 1998], and in turn a locally thick package of strong and continuous reflections, which are interpreted to represent the lower Messinian evaporites ("Gessoso-Solfifera", *Cita and McKenzie* [1986]). The base of this unevenly thick unit is defined by a planar high-amplitude reverse polarity reflector, generally known as B-reflector [Figure 9a; *Finetti and Morelli*, 1973; *Gallais et. al.*, 2011].

The pre-Messinian units are seismically characterized by a succession of high- and low-amplitude, discontinuous reflections that can be correlated to Miocene clastic sediments (Figure 9a). These deposits rest above a planar and continuous reflection, which deepens to the northeast from ~2 to ~5 km. Although this reflection has not been calibrated with well data, based on projection of on-land outcrops [*Van Dijk et al.*, 2000] we interpret it as the top of the Calabrid Paleozoic crystalline rocks and locally overlying Mesozoic-Paleogene deposits (Figure 9a).

Underneath the Amendolara Ridge, the stacked pattern of seismic sequences is more disturbed by thrusting. Some wells north of the ridge (e.g. Lucia and Letizia well, Figure 8) drill through thin imbricates which involves Miocene clastics and evaporites. These sheets, together with their pre-Miocene bedrock (the Ligurid-Sicilid units), form the allochthon thrust wedge, which thickens from northeast to southwest from ~2-2.5 to ~4.5 km beneath the Amendolara Ridge (Figures 10a to 10c).

Beneath and northeast of the Amendolara Ridge, a south-west dipping, continuous and high-amplitude reflection images the top of the Apulia foreland platform which is thrust beneath the allochthonous wedge (Figures 9b, 10a to 10c). The nature of the reflection is proved by the Letizia well (Figure 8), and corresponds to the intra-Messinian unconformity (horizon M) that truncates the pre-Miocene Apulia carbonates [*Butler*, 2009]. This deeper M-reflector is covered by some hundred meters of Pliocene-lower Pleistocene clay and marls (Figure 8), which marks the timing of emplacement of the thrust belt above the Apulia foreland platform.

The Calabrid units on the west, and the Apennines and subjacent Apulia units on the

east meet just under the Amendolara Ridge (Figures 10a to 10c). However, the exact structural relation among these units is not resolved by the available data.

5.4.2. Geometry of Late Pliocene-Quaternary faults

The MCS profiles show that the structure of the Miocene-early Pliocene, northeast-displaced thrust belt is cut by steeper reverse faults which dip both southwest and northeast. The most prominent array, the Amendolara Fault System (AFS; ABFZ in *Ferranti et al.*, 2009), bounds the southern flank of the ridge and is formed by two sub-parallel faults. We name those AF1 and AF2, respectively (Figures 7, 10a to 10c).

Both AF1 and AF2 cut the lower part of the Pliocene-Quaternary unit, and form crustal ramps with a mean dip of ~45°. Note, however, that tracing of the fault becomes uncertain beneath the first ~4 km depth due to poor data quality. Above the ~2 km depth of the ramp upper tip, some low-angle splays branch from both faults where they run through the Messinian evaporite, which provides a preferred detachment level (Figures 10a, 10b).

The vertical throw of the Pliocene-Quaternary sequence that is accommodated by the aggregated fault strands, on the assumption of a planar initial geometry, is estimated at up to ~1.3 km. The amplitude of the overlying fold that deforms the base of the Middle Pleistocene reflector, again on the assumption of a planar original geometry, is ~500-600 m (Figure 10a). These estimates represent maximum bounds.

In map view, the fault array swings following the morphologic separation between highs and lows. West of the Amendolara Bank, the AFS turns and probably merges with an ~east-west striking blind thrust fault bounding the southern side of the structural high drilled by Larissa well (Figures 3b; 7). The non-rectilinear trend of the AFS is mimicked by the pattern of the base Pliocene-Quaternary isobaths, which has maximum depths in the Sibari-Corigliano basin (Figure 7).

An antithetic, southwest-dipping fault, the Valsinni fault system (VFS) is mapped beneath the northern flank of the Amendolara Bank, and is composed of two sub-parallel strands, VF1 and VF2, with a ~300-400 m aggregated throw of the Pliocene-Quaternary sequence (Figure 10a). Toward the north, the VFS limits the structural high drilled by Letizia and Lucia wells (Figure 7), and then projects on-land north of the Pollino Range, where it likely merges with the thrust system located on the northern side of the Valsinni Ridge (Figure 2).

Moving to the southeast, VF1 and VF2 join together and the system comes to a termination, where it is replaced en-echelon by a northeast dipping fault, the Capo Spulico

Fault (CSF, Figures 10b, 10c; note the decreasing displacement and then disappearance of the VFS). The CSF accommodates a throw of the Pliocene-Quaternary base which increases to the southeast up to ~300 m (Figure 10c).

The downward projection of the steeply dipping AFS, VFS and CSF intersects apparent steps within the west-dipping monocline of the Apulia platform as imaged by the deep M-reflector (Figs 10a to 10c). Although the lack of quality data prevents a precise estimate of the offsets in the deep M-reflector, the location and amplitude of the steps in the dipping reflector is broadly consistent with the throw measured on the base Pliocene-Quaternary unit, suggesting that the recent faults cut through the Apulian platform rocks.

In summary, MCS data show that activity on the AFS, VFS and CSF has controlled deformation of the Amendolara Ridge starting from the Late Pliocene (although an earlier Pliocene activity cannot be neglected but is not resolved by data). The upper crustal faults are blind and their upward projection correspond to the broad folds in recent deposits as recorded by the SCS profiles.

5.5. Seismicity analysis

Appraisal of the historic and instrumental seismicity reveals a marked difference between the Lucania Apennines and northern Calabria (Figure 11). Most of the activity is concentrated in the axial part of the Lucania Apennines, but comes to an abrupt termination at the boundary with Calabria. Here, seismic activity is shifted to the east and, although more sparse, covers predominantly the eastern side of the region and its offshore, including a NW-SE trending band in and adjacent to the Amendolara Ridge and Sibari-Corigliano Basin.

Focal mechanisms of earthquakes [*Totaro et al.*, 2013], together with differential geodetic velocities and fault pattern [*Ferranti et al.*, 2014], also suggest active tectonic processes that differ between the two regions. Focal mechanisms in the Lucania Apennines consistently document extension on faults whose strike is parallel to the trend of the belt (Figure 11). Some extensional focal mechanisms are also present in western Calabria. The focal depths of extension-related earthquakes in the western part of Lucania and Calabria are confined to the upper ~15 km of the crust.

In contrast, in the zone of seismicity parallel to the northeast coast of Calabria, focal plane solutions are equally representative of thrust, extensional and strike-slip earthquakes (Figure 11). Thrust and strike-slip earthquakes, which are the most energetic events and thus the more reliable in terms of depth and mechanism, have P-axes oriented between ~NE-SW and ~ESE-WNW. These focal mechanisms are consistent with left-oblique reverse motion on

nodal planes striking NW-SE parallel to the structural trend of the Amendolara Ridge and Sibari-Corigliano Basin. Significantly, the focal depth of these events is on average deeper (10-30 km) than that of the extension-related earthquakes in the hinterland (Figure 11).

Most destructive historical events are located in the axial part of the Apennines and have been associated to causative faults [*DISS Working Group,* 2010]. Notwithstanding, strong and damaging earthquakes have also occurred along the northeastern coast of Calabria and its offshore (e.g. 1836, April 25, with Mw= 6.2; 1917, June 12, with Mw=5.25; 1988, April 13 with Mw=4.4; 2002, April 17 with Mw=4.9; Figure 11), but their sources are yet unknown or debated [*DISS Working Group,* 2010].

6. Fault numerical modeling and slip rate

We compared the expected deformation produced by motion on discrete segments composing the fault arrays with the bathymetry, with horizons U3 (249-270 ka), U5 (430-450 ka) derived from interpretation of the SCS profiles, and with the base of the Middle Pleistocene sequence extracted from MCS profiles.

The starting geometry of the modeled faults was derived from geologic and geophysical datasets presented above. Because of their relatively low resolution, the MCS profiles were only used to obtain a preliminary assessment of fault location, minimum and maximum depth, and dip, that were slightly adjusted during the following iterative comparison between model initial geometry and output. The strike/length of fault segments were derived from the fold map obtained from the SCS dataset (Figure 4a), because of the denser observational constraints and better data quality with respect to the MCS dataset. The width was scaled using empirical relationships with fault length.

Specifically, the modelled geometry of the AFS involves only two segments of fault AF2 underlying the Amendolara and Cariati banks, respectively (Figure 12). This geometry was chosen on the basis of the fold amplitude analysis carried on the SCS profiles, which suggests that structures underneath the intervening Rossano Bank accommodate a transition between the two principal fault segments (Figure 6). This inference is broadly supported by the MCS profile analysis, which indicates lesser cumulative throw for the AFS underneath the Rossano Bank (Figure 10b) with respect to adjacent banks. Based on the above arguments, we consider the Rossano structures as a relay zone linking fault segments underneath the Amendolara and Cariati.

Rakes obtained from published active stress indicators analysis [*Heidbach et al.,* 2008;

Presti et al., 2013] show for this region an ~NE-SW trending Shmax, which averages the observed trend of earthquakes P-axis (Figure 12). The seismologic observation is consistent with fault slip data analysis within the lower Pleistocene Subapennine Clay cropping out along the coast of the Pollino Range [Figure 12; *Ferranti et al.*, 2009]. The NE-SW Shmax adopted here implies left- oblique (rake: 64°-70°) slip on the modeled segments (Table 2).

Modeling results show that the Amendolara Ridge is controlled by steep (45°) blind fault segments that have upper and lower tips between ~2 and ~10 km of depth below sea floor, respectively (Table 2). The anticline below the Amendolara Bank overlies an ~18 km long NE-dipping fault (Amendolara Segment, AS), corresponding to the western part of AF2 identified in the MCS reflection profiles, and an accompanying SW-dipping fault (Valsinni Segment, VS) which broadly coincides with fault VF1 (Figure 10a). In map view, the two faults are slightly oblique (Figure 12), but modeling is consistent with the seismic data and indicates that the southwest-dipping Valsinni Segment merges with the Amendolara Segment at ~7 km depth (Figure 10a). Similarly, the Cariati anticline is underlain by an ~18 km long NE-dipping fault (Cariati Segment, CS) corresponding to the eastern part of fault AF1 (Figures 10c, 12).

We are aware that our interpretation is a best-fit fault model and not, obviously, a real image of the fault, because of the inherent uncertainty in MCS profile interpretation and because of the simplistic results provided by the elastic modelling. The range of dips indicated on the fault model (Figures 10a to 10c) shows the model variability deriving from uncertainty in dip estimation. Similar uncertainties exist on the remaining model parameters (length, rake and so on). What is important here is the general result that current tectonic activity at the Amendolara Ridge is accommodated by reverse fault segments with a left-oblique component of slip.

The input data for calculating the slip rate of fault segments was the growth geometry of seismic units S3 and S5 overlying unconformities U3 and U5, respectively, as imaged in the SCS profiles (Figure 4). We measured the thickness of the sedimentary sequences on the crest of the anticlines and in the synclines (Figures S1a and S1b in the Supplementary Material section; Table 3). The thickness difference between the two locations reflects the relative uplift between anticline and syncline during deposition of the growth strata (i.e. the vertical component of the structural growth according to *Schneider et al.*, [1996]). Where the profile does not reach the axis of the syncline (Figure S1b), the rate is estimated by a downward extrapolation of S5. The slip necessary to produce the estimated relative uplift was calculated using dislocation modeling of the best fitting fault planes. For the sake of

simplicity, in the absence of an estimate for the sedimentation rate, the age of the sequences used to calculate the slip rate was taken as the age of the downward-bounding surface.

In most cases, units S3 and S5 are not continuous over the Amendolara Bank, because they are erosionally truncated by the base of LGM low-stand (S1a in the Supplementary Material section). Nevertheless, the wedge of stacked seismic units thins towards the anticline crest, highlighting that the fold was growing during deposition. Based on these observations, we calculated the slip rate of the Amendolara Segment along the profiles where S3 and S5 were eroded, by assuming a zero thickness over the crest of the anticline. The obtained rate value must be considered as a maximum (Table 3).

It must be noted that the shape of modeled reflectors extracted from the SCS profiles is not entirely structural, because hemipelagic sediments forming the seismic units drape over a pre-existing morphology (Figure S1). In addition, some difference in thickness of seismic units between structural highs and lows can arise from enhanced deposition of sediments in the syncline both from upslope (e.g. gravity flows) and from laterally flowing currents (e. g. contour currents), rather than from a larger accommodation space created by fold growth. To alleviate this latter quandary, we corrected the estimate of structural growth by subtracting, to the thickness of S3 and S5 in the syncline, the thickness of transparent layers (interpreted as gravity flow and/or contourites deposits) mapped on the Sparker profiles (see the sketch in Figure S1a). Where it was not possible to obtain this measurement, we corrected the values adopting an average 15% reduction of growth strata thickness in the basin as estimated from nearby observations (Table 3). In one case the Sparker profiles intercepted what we interpreted to be a fault scarp, which offsets the sea bed and interrupts the continuity of seismic units S5 and S3 (Figures 4f, 5c, and S1c).

The slip rates were not corrected for the effects of differential subsidence induced by consolidation of young, saturated sediments through time. The amount of consolidation is related to the sediment granulometry and is proportional to layer thickness. Hence consolidation effects mimic those of tectonic deformation. *Maesano et al.* [2013], by using a 3D modeling of anticline-syncline fold pairs buried below the Adriatic Sea, estimated that the average thickness change after decompaction may be up to 40% of the original thickness.

Considering the above limitations and uncertainties, the vertical component of the structural growth estimated here must be regarded as a maximum value. However, the existence of fresh, rectilinear sea-bed scarps (Figures 4f, 5c), which were evidently not draped and concealed by sediments, and the progressive tilt of sediment packages lacking evidence of sliding (e. g. Figure 5a to 5c), point to significant structural growth during

deposition.

Modeling results for the Amendolara Segment are strikingly consistent along different profiles for both S5 and S3, with average maximum slip rates of ~0.7-0.8 mm/yr. For the Cariati Segment, slip rates are apparently half (~0.4 mm/yr) of those for the Amendolara Segment. However, as quoted above, the frontal part of the Cariati segment is characterized by a possible fault scarp, with a ~70 m apparent offset of the sea-floor (Fig. 5c). Although we lack markers to compute the fault slip rate, we suggest that the discrepancy in slip rate between the Amendolara and Cariati segments may be taken up by this frontal splay.

When a ~40% decrease (based on the work of *Maesano et al.* [2013]) is applied to the estimated slip rates to account for the lack of decompaction correction for S3 and S5, average slip rates decrease to ~0.4-0.5 mm/yr for both the Amendolara and Cariati (with inclusion of the frontal splay fault) segments.

The average result for the Amendolara Ridge is noticeably similar to the slip rate (0.5 mm/yr) estimated on the base of offset coastal terraces [*Santoro et al.*, 2013] for the modeled Pollino fault segment, the trace of which is west of the Amendolara Segment (Figures 2, 12).

7. Discussion

7.1. Structural model for the Amendolara Ridge.

Integrated analysis of swath bathymetry and seismic profiles with different resolution/penetration shows that the Amendolara Ridge has grown during the late (?) Pliocene-Quaternary as a result of oblique contraction. The various datasets provide independent observations at different spatial and temporal scales that are pivotal in determining the geometry and modes of deformation. Swath mapping of the sea-floor shows that the morphobathymetric pattern is structurally-controlled, and high-resolution SCS profiles reveal that folding has recently occurred at the ridge. The mechanism of deformation is inferred based on the relation between folding and deposition shown in the SCS profiles. Specifically, based on the lack of limb rotation and relatively modest syn-tectonic deposition, a fault-propagation folding model [e.g. *Suppe and Medwedeff*, 1990] can be invoked.

The MCS profiles analysis supports the contention that fold growth imaged by SCS data is related to displacements on underlying blind reverse-oblique faults. The limited resolution of MCS data does not permit an accurate reconstruction of fault geometry at depth, and specifically to what extent faults cut through the interpreted top of the Apulia platform (Figure 10a to 10c). However, modeling of horizons extracted mostly from the high-resolution SCS profiles analysis indicates that fault segments located beneath the Amendolara

and Cariati banks form steep ramps that terminate, and probably merge, at ~9-10 km depth. The Valsinni model segment is linked to the Amendolara segment at ~7 km (Table 2), forming a pop-up like structural culmination.

The modeled faults cut through ~5-6 km of allochthonous sedimentary rocks and their synorogenic cover, plus at least through ~4-5 km of structurally underlying Mesozoic-Cenozoic rocks of the Apulia carbonate platform. Based on well logs and geophysical data from southern peninsular Italy, the sediment thickness in the central part of the Apulia platform is estimated at ~6 km [*Doglioni et al.*, 1999]. It is likely, however, that the sedimentary thickness on this southwest extension of the platform underlying the Amendolara Ridge, toward the ancient Mesozoic continental margin (Figure 1a), was smaller. It is conceivable that the blind fault ramps modeled here merge at or nearb the contact between the sedimentary cover and the pre-Mesozoic crystalline basement of the Adriatic crust. At this depth, the upper crustal faults could continue to cut across the basement as a single crustal ramp, or sole into a diffuse detachment zone (see *Menardi-Noguera and Rea* [2000] and *Scrocca et al.* [2005], for alternative views on the thin- versus thick-skin model for Apulia imbricates beneath the Southern Apennines). Alternatively, the fault segments might be linked into a steeper transcurrent shear zone to form a positive flower structure [e.g. *Van Dijk et al.*, 2000; *Del Ben et al.*, 2007].

The high-angle thrust faults that accommodate imbrication of the Apulia platform beneath the Apennines were possibly primary normal faults, reactivated during late Pliocene-Quaternary shortening [*Butler et al.*, 2004]. Here, we show that steep reverse faults were active beneath the Amendolara Ridge during the same time interval. Although our data resolution does not allow us to propose a robust interpretation, we argue that the AFS was primarily a system of normal faults related in same way to the Mesozoic continental margin (Figure 1a), that were reactivated as oblique-reverse in the late part of the Apenninic orogeny.

7.2. Regional tectonic framework for oblique contraction.

Different models can be invoked to explain the growth, under the Amendolara Ridge, of an oblique-thrust belt. In a first scenario, the ridge could be viewed as part of a regional triangle zone, forming either an active roof duplex kinematically linked to motion on the frontal thrust, or a passive-roof duplex.

On land, the frontal thrust of the Apennines has been inactive since the end of the early Pleistocene [*Patacca and Scandone*, 2007], at a time when the foreland, foredeep and frontal thrust belts started to be uplifted above sea-level [*Ferranti and Oldow*, 2005]. Although more

recent displacement is suspected along the offshore continuation of the front beneath the northern Taranto Gulf [*Butler*, 2009; *Volpi et al.*, 2011], available data do not have the needed resolution to firmly establish post-early Pleistocene motion. Because, as shown here, the Amendolara Ridge faults were active during the entire Pleistocene, lack of motion on the frontal thrust during the same time span would favor a passive-roof duplex model.

A triangle zone scenario is consistent with the analysis of the high-penetration CROP M5 seismic profile located ~100 km southeast and on-strike with the Amendolara Ridge (Figure 1c). The M5 profile shows that the Miocene, east-directed, thin-skinned belt was cut and tilted by deeper back-thrusts, which root in the underthrust Apulia platform. In light of the common structural evolution, the contractional belt highlighted by both *Doglioni et al.* [1999] and in this study would extend for at least ~ 150-200 km above the ancient continental margin (Figure 1a).

In the alternative view that the reverse-oblique faults of the Amendolara Ridge merge down-section into a steep transcurrent zone [*Van Dijk et al.*, 2000; *Del Ben et al.*, 2007], lithospheric processes would play a prominent role. Under this hypothesis, halting of east-directed Adriatic slab retreat coupled with residual southeast Ionian slab roll-back [*D'Agostino et al.*, 2011], and motion of the deep Ionian accretionary prism [*Polonia et al., 2011*], would require transcurrent deformation at the Amendolara Ridge; the upper crustal oblique shortening documented here could result from deep shear along a boundary with irregular morphology [*Reitz and Seeber*, 2012].

The more intriguing scenario that emerges from both models concerns the localization of the deformation belt at the Amendolara Ridge and at its offshore prolongation in the Ionian Sea, because of the existence of a long-lived deep crustal boundary. The Amendolara Ridge, the Sibari-Corigliano Basin, and the backthrust belt of *Doglioni et al.* [1999] all have developed above the transition between the Adriatic continental crust to the north and the Ionian thinned continental or oceanic crust to the south (Figures 1a, 1c). The extreme mechanical interface between crustal sections with different buoyancy might have focused growth of the contractional belt. With Quaternary cessation and slowing of slab roll-back in the Adriatic and Ionian sectors, respectively, convergence between Adria and southern Europe, which is largely accommodated at the seismologically active Dinarides and Albanides front (Figure 1b), could be partly absorbed at the ancient continental margin.

Inversion of earthquake focal mechanisms and fault slip data document an ~NE-SW shortening axis (Figure 12), which implies left-oblique reverse motion on the thrust segments modelled here. Seismologic strain data are consistent with thrust and strike-slip focal

mechanisms just south of the ridge (Figure 11), and the Late Quaternary geologic structure reconstructed using marine geophysical data. The trend of the Shmax in the area is, however, at odds with the NW-SE displacement predicted solely on the base of Adria-Europe interaction [*Carafa and Barba,* 2013]. On the other hand, it is consistent with models invoking shorter-wavelength stress sources, such as those deriving from exploitation of deep crustal heterogeneities, which would rotate the predicted stress toward an ~ENE-WSW trend [*Barba et al.,* 2010; *Pierdominici and Heidbach,* 2012].

7.3. Seismotectonic implications

The fault array defined in the present study is ~50 km long and extends on-land and offshore for several additional tens of km. It is composed of discrete fault segments which underlye individual banks atop the ridge and the surrounding shelf (Figure 12; Table 2). The segmentation, documented by morphobathymetric and high-resolution seismic data, involves, in the part of the system studied here (Figure 12), two main northeast-dipping segments (Amendolara and Cariati faults) linked by a relay ramp (Rossano fault), and a southwest-dipping segment (Valsinni fault). The crustal nature of the segmentation is also suggested by the depositional architecture of the Sibari-Corigliano basin that flanks the AFS on the southern side of the ridge, and whose trend swings mirroring that of the segments of the array (Figure 7). The larger Pliocene-Quaternary sedimentary thickness spatially coincides with the Amendolara segment and Rossano relay, which represents a restraining bend of the array, where syntectonic deposition has been enhanced. The antithetic, southwest-dipping Valsinni segment modeled on the northern side of the Amendolara Ridge controls syn-tectonic deposition in the Amendolara Basin (Figure 7).

According to the size of the three model segments, and following the empirical relationships of *Wells and Coppersmith* [1994], the segments would be able to generate M6+ earthquakes (Table 2). However, there is information on their actual seismic behavior; although we observe that oblique thrusting across the fault system is accompanied by infrequent earthquakess as recorded by seismologic catalogues (Figures 11, S3).

The most energetic, recent earthquake with an epicenter located close to the AFS is the Mw=4.4 1988 event (Figures 11, 12). Although constraints from macroseismic intensities do not provide an accurate epicentral location, we hypothesize that the Mw=5.5 1917 earthquake [*Rovida et al.,* 2011] was also generated along the AFS. Noticeably, the epicenter of both events is located at the western termination of the Cariati segment, and the aftershocks of the 1988 event ceased at the segment boundary (Figure 12). At this location, multibeam (Figure

3a), Sparker (Fig. 4f), and Chirp (Fig. 5c) data highlight an ~50 m sea-floor scarp with low-amplitude reflections. We argue that the scarp reflects an active fault that up-throws older rocks of the bank relative to the basin, and has at least in part formed during multiple co-seismic ruptures. The paleo-earthquakes should have been energetic enough to propagate to the sea-bottom, and thus be characterized by a Mmax close to the 6.3 predicted by the elastic model (Table 2).

Current seismicity indicates activity not at the AFS, instead just south of the fault array (Figures 11 and S3). In particular the Sibari-Corigliano basin shows peaks of relatively high energy release (Figure S3), by using either data from 1981 only (Figure S3a) with re-evaluated magnitude [*Gasperini et al.,* 2013], or a temporal extension of the catalog [*Rovida et al., 2011*; *ISC Bulletin,* 2011] with events from 1600 (Figure S3b) and re-evaluated Mw [*Gasperini et al.,* 2013a,b; *Lolli et al.,* in press]. We hypothesize that this southward shift of the locus of seismicity with respect to the AFS can be an artifact due to a minor azimuthal coverage of the Italian seismic network in the northeastern area, because of the Ionian Sea.

8. Conclusions

Analysis of seismic profiles with different resolution/penetration, and of multibeam swath bathymetry, corroborated by seismicity and regional structural data, indicates that the Amendolara Ridge forms an active tectonic belt at the transition between the Southern Apennines collision belt and the Calabrian subduction forearc. Deformation is expressed by folding of middle-late Pleistocene deposits in response to propagation of underlying blind reverse-oblique, upper crustal fault segments, at an average middle Pleistocene slip rate of ~0.4-0.5 mm/yr.

Although shortening in the frontal part of the Apennines ceased by the middle Pleistocene, and recent motion of the submerged thrust front in the Ionian Sea is not resolved by available data, it appears that a component of contraction may still be ongoing in this more internal region, although at a very slow rate, and with a subdued morphologic signature. The latter limitations encountered in previous analyses have led to the common assumption that this sector of southern Italy is inactive. Our study documents active deformation of young sedimentary deposits and of the sea-floor which, together with assessment of local seismicity, indicates oblique-reverse motion on the fault segments modeled in this study.

Late (?) Pliocene-Quaternary growth of an oblique contractional belt in the study area may be related to a triangle zone behind the submarine thrust front of the Apennines, which was progressively de-activated. Alternatively, it was related to activity of a steep transcurrent

zone, with the blind reverse faults and related fold-propagation folds studied here forming the upper crustal part of a positive flower structure.

The major conclusion of this study is that localization of the deformation belt is controlled by the inherited mechanical interface between the thick Apulian crust and the attenuated Ionian crust. Development of the Amendolara Ridge occurred at a time when halting of Adriatic slab retreat and collision between southern Adria and Europe interacted with a retreating Ionian slab, along an irregular continental margin, that focused left-oblique shortening at the ancient crustal boundary.

Our results are consistent with the deformation pattern recorded by coastal terraces along the Ionian Sea coast of the Apennines. When the two adjoining sectors are considered together, a substantially long (80 km or more) active deformation belt emerges. Appraisal of a deep seismic profile located further offshore the Amendolara Ridge (Figure 1c) brings the total extent of the back-thrust belt to ~180 km. The belt, at least in the part studied here, is segmented, with contrasting geometries and structural styles among the ~15 to 20 km long segments underlying the coast and the banks topping the Amendolara Ridge (Figure 12). Our segmentation model provides a limit to the predicted strain release that, if totally occurring through rupturing, would be capable to generate moderate (M up to 6.3) earthquakes.

Based on numerical modelling, the steep upper crustal fault segments extend at least down to ~10 km depth. Below that depth, they could merge into a steeper deep-seated fault system, a crustal ramp or a detachment zone. It is likely, however, that deformation below the branching depth mostly occurs aseismically and thus simultaneous activation of a substantially longer section of the fault array is unlikely.

Acknowledgments

The Teatioca_2011 expedition was funded by the IAMC (Istituto per l' Ambiente Marino Costiero) CNR, Naples, Italy. The research also benefited from funding from a PRIN 2009-2011 project (responsible C. Monaco). We are very grateful to the commander and crew of the R/V Urania for their skill and cooperation during days spent at sea. The oceanographic cruise could not have been carried out without the diligent work of many researchers and graduate students from various institutions. The careful review of Alina Polonia, Marc-Andre Gutscher, Nano Seeber and an anonymous reviewer greatly improved the quality of the paper. Data used in this paper are available via request to Authors.

References

Barnes, P. M., and A. Nicol (2004), Formation of an active thrust triangle zone associated with structural inversion in a subduction setting, eastern New Zealand, *Tectonics*, 23(1), TC1015, doi:10.1029/2002TC001449.

Bigi, G., G. Bonardini, R. Catalano, D. Cosentino, F. Lentini, M. Parotto, R. Sartori, P. Scandone, and E. Turco (1992), Structural Model of Italy, 1:500.000. National Research Council - Consiglio Nazionale delle Ricerche (CNR), Rome.

Butler, R. W. H., S. Mazzoli, S. Corrado, M. De Donatis, D. Di Bucci, R. Gambini, G. Naso, C. Nicolai, D. Scrocca, P. Shiner, and V. Zucconi (2004) Applying thick-skinned tectonic models to the Apennine thrust belt of Italy—Limitations and implications, in K. R. McClay, ed., Thrust tectonics and hydrocarbon systems: *AAPG Memoir*, 82, 647–667.

Butler, R. W. H. (2009), Relationships between the Apennine thrust belt, foredeep and foreland revealed by marine seismic data, offshore Calabria, *Ital. J. Geosci.*, 128(2), 269-278, doi:10.3301/IJG.2009.128.2.269.

Capozzi, R., A. Artoni, L. Torelli, S. Lorenzini, D. Oppo, P. Mussoni, and A. Polonia (2012), Neogene to Quaternary tectonics and mud diapirism in the Gulf of Squillace (Crotone-Spartivento Basin, Calabrian Arc, Italy), *Mar. Petr. Geol.*, 35(1), 219-234, doi:10.1016/j.marpetgeo.2012.01.007.

Caputo, R., M. Bianca, and R. D'Onofrio (2010), Ionian marine terraces of Southern Italy: Insights into the Quaternary tectonic evolution of the area, *Tectonics*, 29, TC4005, doi:10.1029/2009TC002625.

Carafa, M. M. C., and S. Barba (2011), Determining rheology from deformation data: The case of central Italy, Tectonics, 30, TC2003, doi:10.1029/2010TC002680.

Catalano, S., C. Monaco, L. Tortorici, and C. Tansi (1993), Pleistocene strike-slip tectonics in the Lucanian Apennine (Southern Italy), *Tectonics*, 12(3), 656–665, doi:10.1029/92TC02251.

Catalano, R., C. Doglioni, and S. Merlini (2001), On the Mesozoic Ionian Basin, *Geophys. J. Int.*, 144, 49–64, doi:10.1046/j.0956-540X.2000.01287.X.

Cavazza, W., and P. G. DeCelles (1998), Upper Messinian siliciclastic rocks in southeastern Calabria (southern Italy): palaeotectonic and eustatic implications for the evolution of the central Mediterranean region, *Tectonophysics*, 298(1–3), 223–241, doi:10.1016/S0040-1951(98)00186-3.

Cita, M. B., and J. A. McKenzie (1986), The terminal Miocene event, in: Hsu, K.J. (Ed.),

Mesozoic and Cenozoic Oceans, AGU, *Geodyn. Ser.*, 15, 123–140.

Cormier, M.H., L. Seeber, C. McHugh, A. Polonia, M.N. Çag˘atay, O. Emre, L. Gasperini, N. Görür, G. Bortoluzzi, E. Bonatti, W.B.F. Ryan, and K.R. Newman (2006), North Anatolian Fault in the Gulf of Izmit (Turkey): Rapid vertical motion in response to minor bends of a nonvertical continental transform, *J. Geophys. Res.*, 111, B04102, doi:10.1029/2005JB003633.

CPTI Working Group (2004). Catalogo Parametrico dei Terremoti Italiani (CPTI04), on-line publication at http://emidius.mi.ingv.it/CPTI04/presentazione.html (in Italian).

CSTI 1.0 Working Group (2001), "Catalogo strumentale dei terremoti italiani dal 1981 al 1996", Version 1.0 ISBN 88-491-1734-5 Clueb Bologna, available from: http://csi.rm.ingv.it/ (last accessed 19 december 2013).

Cucci, L., and F. R. Cinti (1998), Regional uplift and local tectonic deformation recorded by the Quaternary marine terraces on the Ionian coast of northern Calabria (southern Italy), *Tectonophysics*, 292(1–2), 67–83, doi:10.1016/S0040-1951(98)00061-4.

D'Agostino, N., E. D'Anastasio, A. Gervasi, I. Guerra, M. R. Nedimović, L. Seeber, and M. Steckler (2011), Forearc extension and slow rollback of the Calabrian Arc from GPS measurements, *Geophys. Res. Lett.*, 38, L17304, doi:10.1029/2011GL048270.

de Voogd, B., C. Truffert, N. Chamot-Rooke, P. Huchon, S. Lallemant, and X. Le Pichon (1992), Two-ship deep seismic soundings in the basins of the eastern Mediterranean Sea (Pasiphae cruise), Geophys. J. Int., 109, 536–552, doi:10.1111/ j.1365-246X.1992.tb00116.x.

Del Ben, A., C. Barnaba, and A. Toboga (2007), Strike-slip systems as the main tectonic features in the Plio-Quaternary kinematics of the Calabrian Arc, *Mar. Geophys. Res.*, 29(1), 1–12, doi:10.1007/s11001-007-9041-6.

Di Bucci, D., D. Ridente, U. Fracassi, F. Trincardi, and G. Valensise (2009), Marine palaeoseismology from very high resolution seismic imaging: The Gondola Fault Zone (Adriatic foreland), *Terra Nova*, 21, 393–400, doi:10.1111/j.1365-3121.2009.00895.x.

DISS Working Group (2010), Database of Individual Seismogenic Sources (DISS), Version 3.1.1: A compilation of potential sources for earthquakes larger than M 5.5 in Italy and surrounding areas. http://diss.rm.ingv.it/diss/, © INGV 2010 - Istituto Nazionale di Geofisica e Vulcanologia - All rights reserved; doi:10.6092/INGV.IT-DISS3.1.1.

Doglioni, C., S. Merlini, G. Cantarella (1999), Foredeep geometries at the front of the Apennines in the Ionian Sea (central Mediterranean), *Earth Planet. Sci. Lett.*, 168, 243–254, doi: 10.1016/S0012-821X(99)00059-X.

Dziewonski, A. M., T.-A. Chou, and J. H. Woodhouse (1981), Determination of earthquake source parameters from waveform data for studies of global and regional seismicity, *J. Geophys. Res.*, 86(B4), 2825–2852, doi:10.1029/JB086iB04p02825.

Earthquake mechanisms of the Mediterranean Area (EMMA), http://ibogfs.df.unibo.it/user2/paolo/www/ATLAS/pages/EMMA_description.htm

Faccenna, C., T. W. Becker, F. P. Lucente, L. Jolivet, and F. Rossetti (2001), History of subduction and back-arc extension in the Central Mediterranean, *Geophys. J. Int.*, 145(3), 809–820, doi:10.1046/j.0956-540x.2001.01435.X.

Ferranti L, and J.S. Oldow (2005), Latest Miocene to Quaternary horizontal and vertical displacement rates during simultaneous contraction and extension in the Southern Apennines orogen, Italy. *Terra Nova*, 17, 209-214.

Ferranti, L., E. Santoro, M. E. Mazzella, C. Monaco, and D. Morelli (2009), Active transpression in the northern Calabria Apennines, southern Italy, *Tectonophysics*, 476(1–2), 226–251, doi:10.1016/j.tecto.2008.11.010.

Ferranti, L., M. Palano, F. Cannavò, M.E. Mazzella, J. S. Oldow, E. Gueguen, M. Mattia, and C. Monaco (2014), Rates of geodetic deformation across active faults in southern Italy. *Tectonophysics*, 621 (2014) 101–122, http://dx.doi.org/10.1016/j.tecto.2014.02.007.

Finetti, I., and C. Morelli (1973), Geophysical exploration of the Mediterranean Sea, *Boll. Geofis. Teor. Appl.*, 14, 263–340.

Gallais, F., M.-A. Gutscher, D. Graindorge, N. Chamot-Rooke, and D. Klaeschen (2011), A Miocene tectonic inversion in the Ionian Sea (central Mediterranean): Evidence from multichannel seismic data, J. Geophys. Res., 116, B12108, doi:10.1029/2011JB008505.

Gasperini, P., B. Lolli, G. Vannucci, and E. Boschi (2012), Calibration of moment magnitude estimates for the European-Mediterranean and Italian regions, *Geophys. J. Int.*, 190, 1733–1745, doi: 10.1111/j.1365-246X.2012.05575.x.

Gasperini, P., B. Lolli, and G. Vannucci (2013), Empirical calibration of Local Magnitude data sets versus Moment Magnitude in Italy, *Bull. Seism. Soc. Am.*, 103(4), 2227–2246, doi:10.1785/0120120356.

Gasperini, P., B. Lolli, and G. Vannucci (2013b), Body wave magnitude mb is a good proxy of moment magnitude Mw for small earthquakes (mb<4.5-5.0), *Seism. Res. Lett.* 84, 6, 932-937, doi: 10.1785/0220130105.

Goldfinger, C., et al. (2012), Turbidite Event History: Methods and Implications for Holocene Paleoseismicity of the Cascadia Subduction Zone, U.S. Geological Survey Professional Paper 1661-F, 184 pp., 64 figures, U.S. Geological Survey, Reston, Va.

http://pubs.usgs.gov/pp/pp1661f.

Gueguen, E., C. Doglioni, and M. Fernandez (1998), On the post-25 Ma geodynamic evolution of the western Mediterranean, *Tectonophysics*, 298, 259–269, doi:10.1016/S0040-1951(98)00189-9.

Heidbach, O., M. Tingay, A. Barth, J. Reinecker, D. Kurfeß, and B. Müller (2008), The World Stress Map database release 2008, doi:10.1594/GFZ.WSM.Rel2008, 2008.

Hippolyte, J. C., J. Angelier, and F. Roure (1994), A major geodynamic change revealed by Quaternary stress patterns in the Southern Apennines (Italy), *Tectonophysics*, 230(3–4), 199–210, doi:10.1016/0040-1951(94)90135-X.

International Seismological Centre – ISC Bulletin (2011), On-line Bulletin, http://www.isc.ac.uk, Internatl. Seis. Cent., Thatcham, United Kingdom, 2011.

Jouanne, F., J.L. Mugnier, R. Koci, S. Bushati, K. Matev, N. Kuka, I. Shinko, S. Kociu, and L. Duni (2012), GPS constraints on current tectonics of Albania, *Tectonophysics*, 554–557, 50–62.

Kanamori, H. (1971), Great earthquakes at island arcs and lithosphere, Tectonophysics, 12, 187-1323, doi:10.1016/0040-1951(71)90003-5.

Lambeck, K., F. Antonioli, M. Anzidei, L. Ferranti, G. Leoni, and S. Silenzi (2011), Sea level change along the Italian coasts during Holocene and prediction for the future, *Quat. Int.*, 232(1–2), 250–257, doi:10.1016/j.quaint.2010.04.026.

Lisiecki, L. E., and M. E. Raymo (2005), A Pliocene-Pleistocene stack of 57 globally distributed benthic d18O records, *Paleoceanography*, 20, PA1003, doi:10.1029/2004PA001071.

Lolli, B., P. Gasperini, and G. Vannucci (in press), Empirical conversion between teleseismic magnitudes (mb and Ms) and moment magnitude (Mw) at the Global, Euro-Mediterranean and Italian scale, *Geophys. J. Int* (GJI-13-0733.R3).

Maesano, F. E., G. Toscani, P. Burrato, F. Mirabella, C. D'Ambrogi, and R. Basili (2013), Deriving thrust fault slip rates from geological modeling: Examples from the Marche coastal and offshore contraction belt, Northern Apennines, Italy, *J. Mar. Petr. Geol.*, 42, 122-134, doi:10.1016/j.marpetgeo.2012.10.008.

Malinverno, A., M. Cafiero, W. B. F. Ryan, and M. B. Cita (1981), Distribution of Messinian sediments and erosional surfaces beneath the Tyrrhenian Sea: geodynamic implications, *Oceanol. Acta*, 4, 489-496.

Malinverno, A., and W. B. F. Ryan (1986), Extension in the Tyrrhenian Sea and shortening in the Apennines as a result of arc migration driven by sinking of the lithosphere,

Tectonics, 5(2), 227–245, doi:10.1029/TC005i002p00227.

Menardi-Noguera, A., and G. Rea (2000), Deep structure of the Campanian–Lucanian Arc (Southern Apennine, Italy), *Tectonophysics*, 324(4), 239–265, doi:10.1016/S0040-1951(00)00137-2.

Minelli, L., and C. Faccenna (2010), Evolution of the Calabrian accretionary wedge (central Mediterranean), Tectonics, 29, TC4004, doi:10.1029/2009TC002562.

Monaco, C., L. Tortorici, and W. Paltrinieri (1998), Structural evolution of the Lucanian Apennines, southern Italy, *J. Struct. Geol.*, 20(5), 617–638, doi:10.1016/S0191-8141(97)00105-3.

Nicol, A., P. A. Gillespie, C. Childs, and J. J. Walsh (2002), Relay zones between mesoscopic thrust faults in layered sedimentary sequences, *J. Struct. Geol.*, 24(4), 709–727, doi:10.1016/S0191-8141(01)00113-4.

Nicolai, C., and R. Gambini (2007), Structural architecture of the Adria platform-and-basin system, *Boll. Soc. Geol. It.*, Spec. Issue 7(2007), 21-37; Mazzotti, A., E. Patacca, and P. Scandone (Eds), "Results of the CROP Project, Sub-project CROP-04.

Nodder, S. D., G. Lamarche, J.-N. Proust, and M. Stirling (2007), Characterizing earthquake recurrence parameters for offshore faults in the low-strain, compressional Kapiti-Manawatu Fault System, New Zealand, *J. Geophys. Res.*, 112, B12102, doi:10.1029/2007JB005019.

Okada, Y. (1985), Surface deformation due to shear and tensile faults in a half-space, *Bull. Seismol. Soc. Am.*, 75(4), 1135–1154.

Okamura, Y., K. Satake, K. Ikehara, A. Takeuchi, and K. Arai (2005), Paleoseismology of deep-sea faults based on marine surveys of northern Okushiri ridge in the Japan Sea, *J. Geophys. Res.*, 110, B09105, doi:10.1029/2004JB003135.

Papanikolaou, I. D., and G. P. Roberts (2007), Geometry, kinematics and deformation rates along the active normal fault system in the southern Apennines: Implication for fault growth, *J. Struct. Geol.*, 29(1), 166–188, doi:10.1016/j.jsg.2006.07.009.

Patacca, E., R. Sartori, and P. Scandone (1990), Tyrrhenian Basin and Apenninic arcs: Kinematic relations since late Tortonian times, *Mem. Soc. Geol. Ital.*, 45, 425–451.

Patacca E., and P. Scandone (2007), Geology of the Southern Apennines, *Boll. Soc. Geol. It.*, Spec. Issue 7(2007), 75-119; Mazzotti, A., E. Patacca, and P. Scandone (Eds), "Results of the CROP Project, Sub-project CROP-04.

Pepe F., A. Sulli, G. Bertotti, and F. Cella (2010), Architecture and Neogene to Recent evolution of the western Calabrian continental margin: An upper plate perspective to

the Ionian subduction system, central Mediterranean. *Tectonics*, 29, TC3007, doi:10.1029/2009TC002599.

Pepe, F., A. Sulli, M. Agate, D. Di Maio, A. Kok, C. Lo Iacono, and R. Catalano (2003), Plio–Pleistocene geological evolution of the northern Sicily continental margin (southern Tyrrhenian Sea): new insights from high-resolution, multi-electrode sparker profiles, *Geo-marine Letters*, 23(1), 53–63, doi: 10.1007/s00367-003-0124-3.

Pepe, F., G. Bertotti, L. Ferranti, M. Sacchi, A.M. Collura, S. Passaro, and A. Sulli (2014), Pattern and rate of post-20 ka vertical tectonic motion around the Capo Vaticano Promontory (W Calabria, Italy) based on offshore geomorphological indicators, *Quaternary International* (2013), http://dx.doi.org/10.1016/ j.quaint.2013.11.012

Pierdominici, S., and O. Heidbach (2012), Stress field of Italy - Mean stress orientation at different depths and wave-length of the stress pattern, *Tectonophysics*, 532-535, 301–311, doi:10.1016/j.tecto.2012.02.018.

Polonia, A., L. Torelli, P. Mussoni, L. Gasperini, A. Artoni, and D. Klaeschen (2011), The Calabrian Arc subduction complex in the Ionian Sea: Regional architecture, active deformation, and seismic hazard, Tectonics, 30, TC5018, doi:10.1029/2010TC002821.

Polonia A., L. Torelli, L. Gasperini, and P. Mussoni (2012), Active faults and historical earthquakes in the Ionian Sea, Nat. Hazards Earth Syst. Sci., 12, 2311–2328. http://www.nat-hazards-earth-syst-sci.net/12/2311/2012/ doi:10.5194/nhess-12-2311-2012.

Pondrelli, S., A. Morelli, G. Ekström, S. Mazza, E. Boschi, and A.M. Dziewonski (2002), European-Mediterranean regional centroid-moment tensors: 1997–2000, *Phys. Earth Planet. Int.*, 130, 71–101, doi:10.1016/S0031-9201(01)00312-0.

Pondrelli S., S. Salimbeni, G. Ekström, A. Morelli, P. Gasperini, and G. Vannucci (2006), The Italian CMT dataset from 1977 to the present, *Phys. Earth Planet. Int.*, 159 (3-4), 286-303, doi:10.1016/j.pepi.2006.07.008.

Pondrelli, S., S. Salimbeni, A. Morelli, G. Ekström, L. Postpischl, G. Vannucci, and E. Boschi (2011), European–Mediterranean Regional Centroid Moment Tensor catalog: Solutions for 2005–2008, *Phys. Earth Plan. Int.*, 185, 74-81, doi:10.1016/j.pepi.2011.01.007.

Presti, D., A. Billi, B. Orecchio, C. Totaro, C. Faccenna, and G. Neri (2013), Earthquake focal mechanisms, seismogenic stress, and seismotectonics of the Calabrian Arc, Italy, *Tectonophysics*, 602, 153-175, doi:10.1016/j.tecto.2013.01.030.

Reitz, M. A., and L. Seeber (2012), Arc-parallel strain in a short rollback-subduction system:

The structural evolution of the Crotone basin (northeastern Calabria, southern Italy), *Tectonics*, 31, TC4017, doi:10.1029/2011TC003031.

Ridente, D., and F. Trincardi (2002), Eustatic and tectonic control on deposition and lateral variability of Quaternary regressive sequences in the Adriatic basin (Italy), *Mar. Geol.*, 184(3-4), 273-293, doi:10.1016/S0025-3227(01)00296-1.

Roure, F., P. Casero, and R. Vially (1991), Growth processes and melange formation in the southern Apennines accretionary wedge, *Earth Plan. Sci. Lett.*, 102, 395-412, doi:10.1016/0012-821X(91)90031-C.

Rovida, A., R. Camassi, P. Gasperini, and M. Stucchi (Eds.) (2011), CPTI11, the 2011 version of the Parametric Catalogue of Italian Earthquakes. Milano, Bologna, http://emidius.mi.ingv.it/CPTI, DOI: 10.6092/INGV.IT-CPTI11.

Ryan, W. B. F. (1969), Decoding the Mediterranean salinity crisis, *Sedimentology*, 56, 95–136, doi:10.1111/j.1365-3091.2008.01031.x.

Santoro, E., M. E. Mazzella, L. Ferranti, A. Randisi, and E. Napolitano (2009), Raised coastal terraces along the Ionian Sea coast of northern Calabria, Italy, suggest space and time variability of tectonic uplift rates, *Quat. Int.*, 206, 78–101, doi:10.1016/j.quaint.2008.10.003.

Santoro, E., L. Ferranti, P. Burrato, M. E. Mazzella, and C. Monaco (2013), Deformed Pleistocene marine terraces along the Ionian Sea margin of southern Italy: Unveiling blind fault-related folds contribution to coastal uplift, *Tectonics*, 32, doi:10.1002/tect.20036.

Schneider, C. L., C. Hummon, R. S. Yeats, and G. L. Huftile (1996), Structural evolution of the northern Los Angeles basin, California, based on growth strata, *Tectonics*, 15(2), 341-355, doi:10.1029/95TC02523.

Scognamiglio, L., E. Tinti, and A. Michelini (2009), Real-Time determination of seismic moment tensor for the Italian region, *Bull. Seismol. Soc. Am.*, 99, 2223–2242, doi:10.1785/0120080104.

Scrocca, D., E. Carminati, and C. Doglioni (2005), Deep structure of the southern Apennines, Italy: Thin-skinned or thick-skinned? *Tectonics*, 24, TC3005, doi:10.1029/2004TC001634.

Senatore, M.R, W.R. Normark, T, Pescatore, and S. Rossi (1988), Structural framework of the Gulf of Taranto (Ionian Sea), *Bollettino della Società Geologica Italiana*, 41, 533–539.

Serpelloni, E., G. Vannucci, S. Pondrelli, A. Argnani, G. Casula, M. Anzidei, P. Baldi, and P.

Gasperini (2007), Kinematics of theWestern Africa-Eurasia plate boundary from focal mechanisms and GPS data, *Geophys. J. Int.*, 169, 1180–1200, doi:10.1111/j.1365-246X.2007.03367.x.

Spina, V., E. Tondi, P. Galli, and S. Mazzoli (2009), Fault propagation in a seismic gap area (northern Calabria, Italy): Implications for seismic hazard, *Tectonophysics*, 476, 357–369, doi:10.1016/j.tecto.2009.02.001.

Suppe, J., and D. Medwedeff (1990), Geometry and kinematics of fault-propagation folding, *Eclogae Geologicae Helvetiae*, 83(3), 409-454.

Totaro, C., D. Presti, A. Billi, A. Gervasi, B. Orecchio, I. Guerra, and G. Neri (2013), The ongoing seismic sequence at the Pollino Mountains, Italy. *Seismol. Res. Lett*. 84 (6), 955–962. http://dx.doi.org/10.1785/0220120194.

Van Dijk, J. P., M. Bello, G. P. Brancaleoni, G. Cantarella, V. Costa, A. Frixa, F. Golfetto, S. Merlini, M. Riva, S. Torricelli, C. Toscano, and A. Zerilli (2000), A regional structural model for the northern sector of the Calabrian Arc (southern Italy), *Tectonophysics*, 324(4), 267–320, doi:10.1016/S0040-1951(00)00139-6.

Vannucci, G., and P. Gasperini (2003), A database of revised fault plane solutions for Italy and surrounding regions, *Comput. Geosciences*, 29, 903–909.

Vannucci, G. and P. Gasperini (2004), The new release of the database of earthquake mechanisms of the Mediterranean area (EMMA Version 2), *Ann. Geophys.*, 47, 307–334.

Vannucci G., P. Imprescia, and P.Gasperini (2010), deliverable n. 2 of the UR2.05 in the INGV-DPC S1 project (2007-2009). INGV-DPC Internal report and database.

Volpi V., D. Accettella, and A. Cuppari (2011), Morphological features of the Apennines foreland/accretionarywedge boundary in the Ionian Sea. Marine Geophysical Research, 32, 481–492, doi:10.1007/s11001-011-9140-2.

Waelbroeck, C., L. Labeyrie, E. Michel, J. C. Duplessy, K. Lambeck, J. F. McManus, E. Balbon, and M. Labracherie (2002), Sea-level and deep water temperature changes derived from benthic foraminifera isotopic records, *Quat. Sci. Rev.*, 21(1–3), 295–305, doi:10.1016/S0277-3791(01)00101-9.

Wells, D. L., and K. J. Coppersmith (1994), New empirical relationships among magnitude, rupture length, rupture width, rupture area, and surface displacement, *Bull. Seismol. Soc. Am.*, 84(4), 974–1002.

Westaway, R. (1993), Quaternary uplift of southern Italy, *J. Geophys. Res.*, 98(B12), 21741–21772, doi:10.1029/93JB01566.

Table 1: Seismic units and bounding surfaces on the Sparker seismic profiles.

Seismic unit	Surface	MIS	Surface Age (ka)	Age source
S1	sea-floor			
S2	U1	2	18-23	*Waelbroeck et al.* [2002]
S3	U2	6	137-150	*Waelbroeck et al.* [2002]
S4	U3	8	249-270	*Waelbroeck et al.* [2002]
S5	U4	10	343-345	*Waelbroeck et al.* [2002]
S6	U5	12	430-450	*Waelbroeck et al.* [2002]
S7	U6	14	530-550	*Lisiecki and Raymo* [2005]
S8	U7	16	630-650	*Lisiecki and Raymo* [2005]
S9	U8	18	710-720	*Lisiecki and Raymo* [2005]
	U9	20	800	*Lisiecki and Raymo* [2005]

[a]

Table 1. Seismic units and relative bounding surfaces recognized on the Sparker seismic profiles. Each seismic unit is bounded on top and bottom by the corresponding surfaces, respectively, as listed in the related column. The assigned correlation with individual Marine Isotope Stage (MIS) is also shown.

Table 2. Geometrical parameters of individual thrusts from dislocation modeling

Name	Strike	Dip	Rake	Length	Width	Minimum depth (km)	Maximum depth (km)	expected Magnitude
Amendolara segment	298	45	64	17.5	9.5	2.0	8.7	6.3
Cariati segment	298	45	65	18	9.7	1.5	8.4	6.3
Valsinni segment	128	45	70	11.3	7.0	2.0	6.9	6.1

Table 2: Geometric and kinematic parameters of the fault segments underlying the Amendolara Ridge modeled in this study. The expected magnitude of each segment was derived from the empirical relationships of *Wells and Coppersmith* [1994].

Table 3. Slip rates of the thrust segments calculated in this study

Fault segment	Sparker line	marker	Age ka	relative uplift m	slip m	slip rate mm/a	relative uplift m corrected [3]	slip m corrected [3]	slip rate mm/a corrected	Notes
Amendolara Segment	Tea_15	U5	450 - 430	185	434	0.97-1.01			0.82-0.86[4]	
	Tea_30		450 - 430	182[1]	386	0.86-0.90	163	344	0.77-0.80[3]	maximum value, U5 eroded on top of anticline
	Tea_9		450 - 430	181[1]	391	0.87-0.91			0.74-0.77[4]	maximum value, U5 eroded on top of anticline
	Tea_32		450 - 430	117[1, 2]	247	0.55-0.58	97	205	0.46-0.48[3]	maximum value, U5 eroded on top of anticline
	Tea_17		450 - 430	187	412	0.92-0.96	163	359	0.80-0.83[3]	
	Tea_15	U3	270 - 249	155[1]	364	1.35-1.46			1.15-1.24[4]	maximum value, U3 eroded on top of anticline
	Tea_17		270 - 249	86[1]	189	0.70-0.76	63	139	0.51-0.56[3]	maximum value, U3 eroded on top of anticline
	Tea_30		270 - 249	125[1]	265	0.98-1.06	106	225	0.83-0.90[3]	maximum value, U3 eroded on top of anticline
	Tea_9		270 - 249	130[1]	281	1.04-1.13			0.88-.096[4]	maximum value, U3 eroded on top of anticline
	Tea_32		270 - 249	106[1]	224	0.83-0.90	86	182	0.67-0.73[3]	maximum value, U3 eroded on top of anticline
Cariati Segment	Tea_3b	U5	450 - 430	93	231	0.51-0.54			0.44-0.46[4]	

Tea_5	450 - 430	59	14 8	0.55-0.59		0.47-0.51[4]

Table 3: Slip rates of the Amendolara and Cariati thrust fault segments calculated from simple dislocation modeling using growth strata identified in the Sparker lines. Ages of the deformed markers are taken from *Waelbroeck et al.* [2002], see Table 1. (1) Maximum relative uplift considering no deposition of S3 or S5 over the anticline and not considering LGM low-stand erosion. (2) Value obtained with a linear interpolation of the thickness change of seismic unit S5 in the syncline. (3) Values corrected subtracting the measured thickness of debris flow deposits from the geometry of growth strata (on average 10-15% of the original value). (4) Values corrected subtracting an estimated average thickness (15% of the original value) of debris flow deposits from the geometry of growth strata in the syncline.

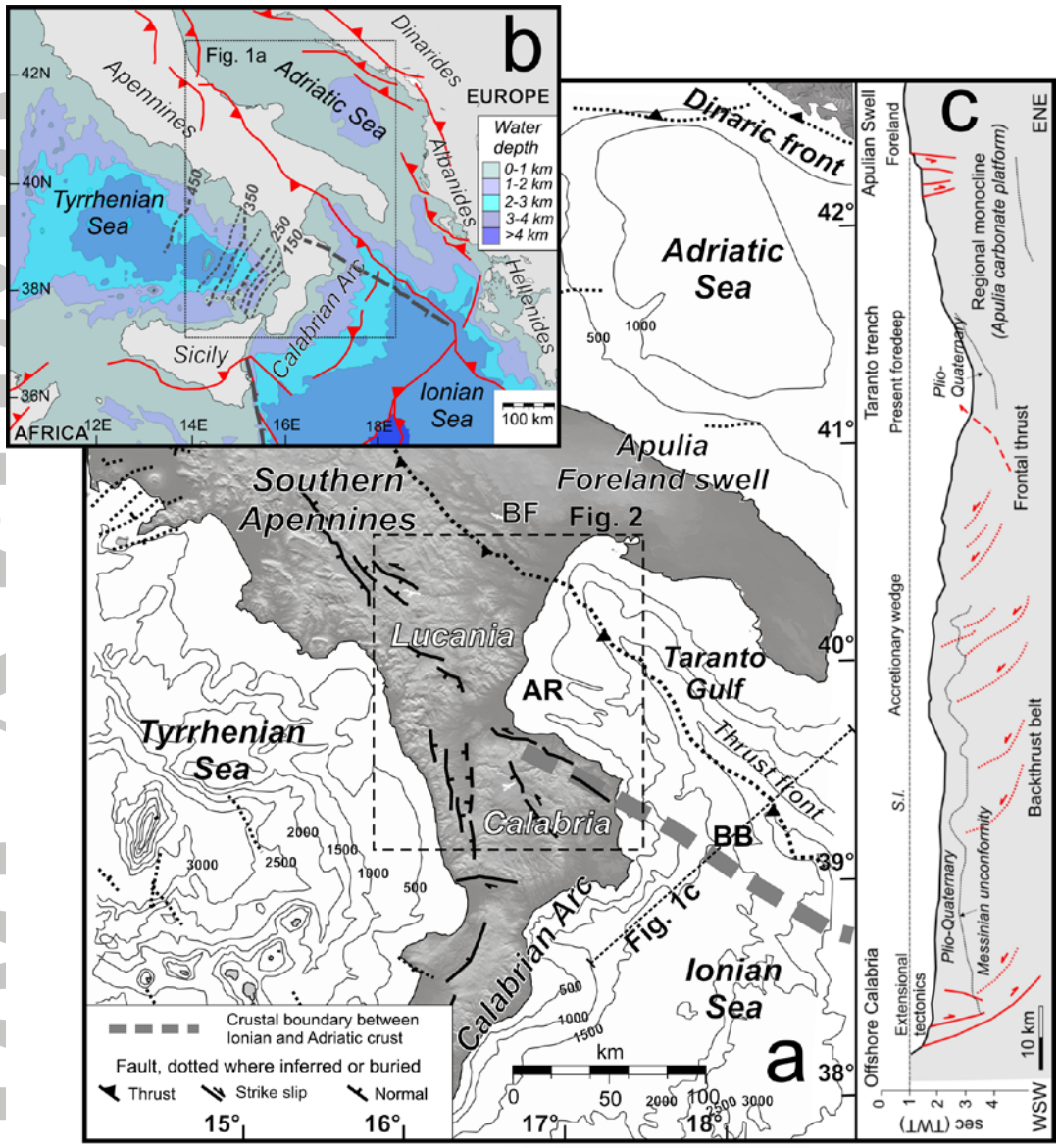

Figure 1. Regional tectonic setting of southern Italy. (a) Tectonic map showing the Apulian swell, the Southern Apennines and Calabrian arc orogens, the front of the thin-skinned thrust belt of the Apennines, the deep transition between Ionian and Apulian crusts (after *Catalano et al.* [2001]), and the main active faults on land and offshore (after *Ferranti et al.* [2009]). AR, Amendolara Ridge; BF, Bradano Foredeep basin; BB, backthrust belt of *Doglioni et al.* [1999] (Figure 1c). b) Geodynamic setting of the central Mediterranean, showing the regional contractional structures; dotted lines are isobaths of the Ionian slab (from *D'Agostino et al.*, [2011]), thicker dashed lines are the conjugate continental margins of the Ionian Sea (after *Catalano et al.* [2001]). c) Line-drawing of deep crustal profile CROP M5 (after *Doglioni et al.* [1999]), whose trace is in Figure 1a.

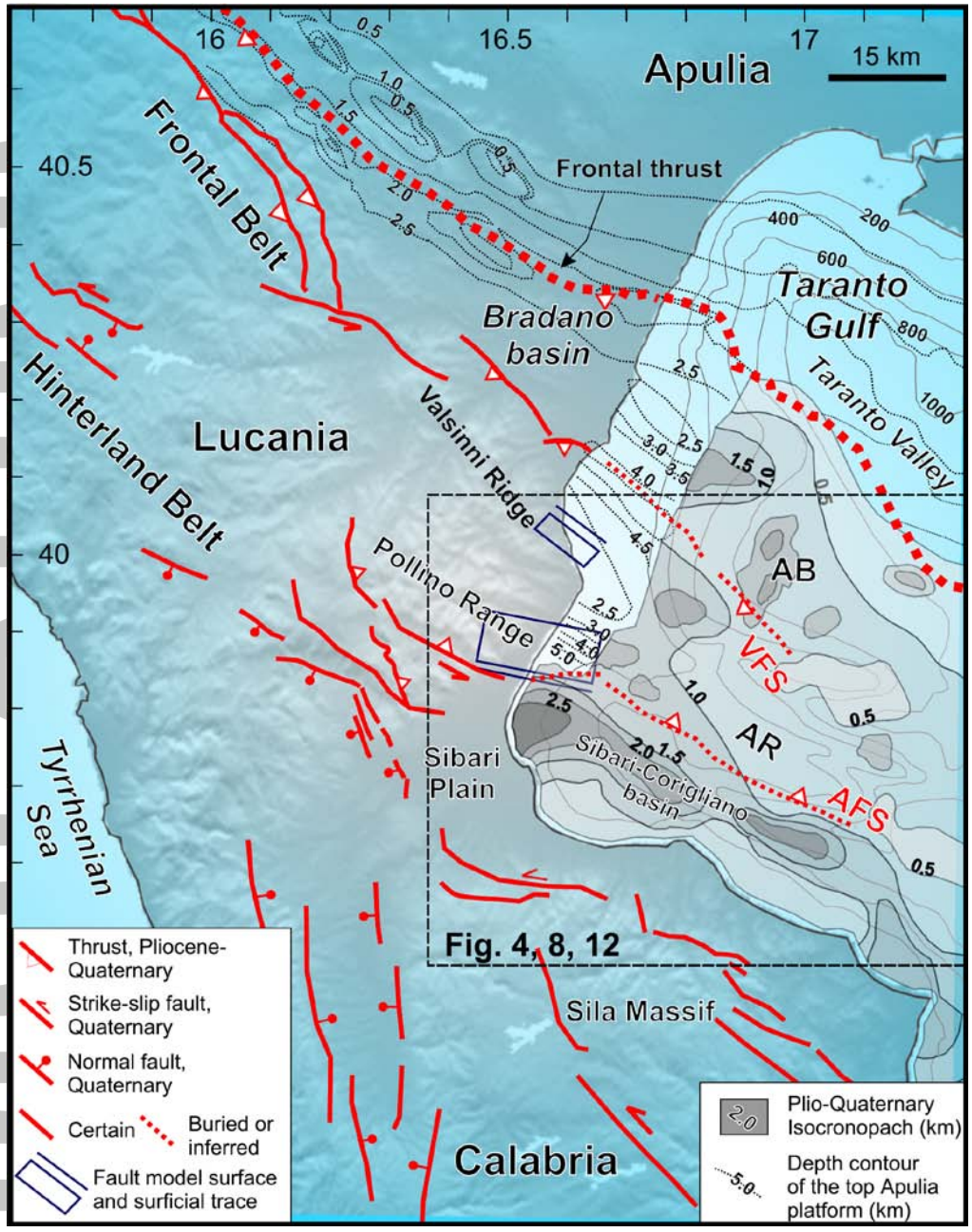

Figure 2. Tectonic map of the Southern Apennines frontal zone in southern Lucania and northern Calabria. Pliocene-Quaternary isochronopachs and depth to the top of the Apulia platform from *Bigi et al.* [1992]. Boxes are thrust segments derived from dislocation modeling by *Santoro et al.* [2013]. Amendolara Fault System (AFS) and Valsinni Fault System (VFS) from this work. AR, Amendolara Ridge; AB, Amendolara Basin.

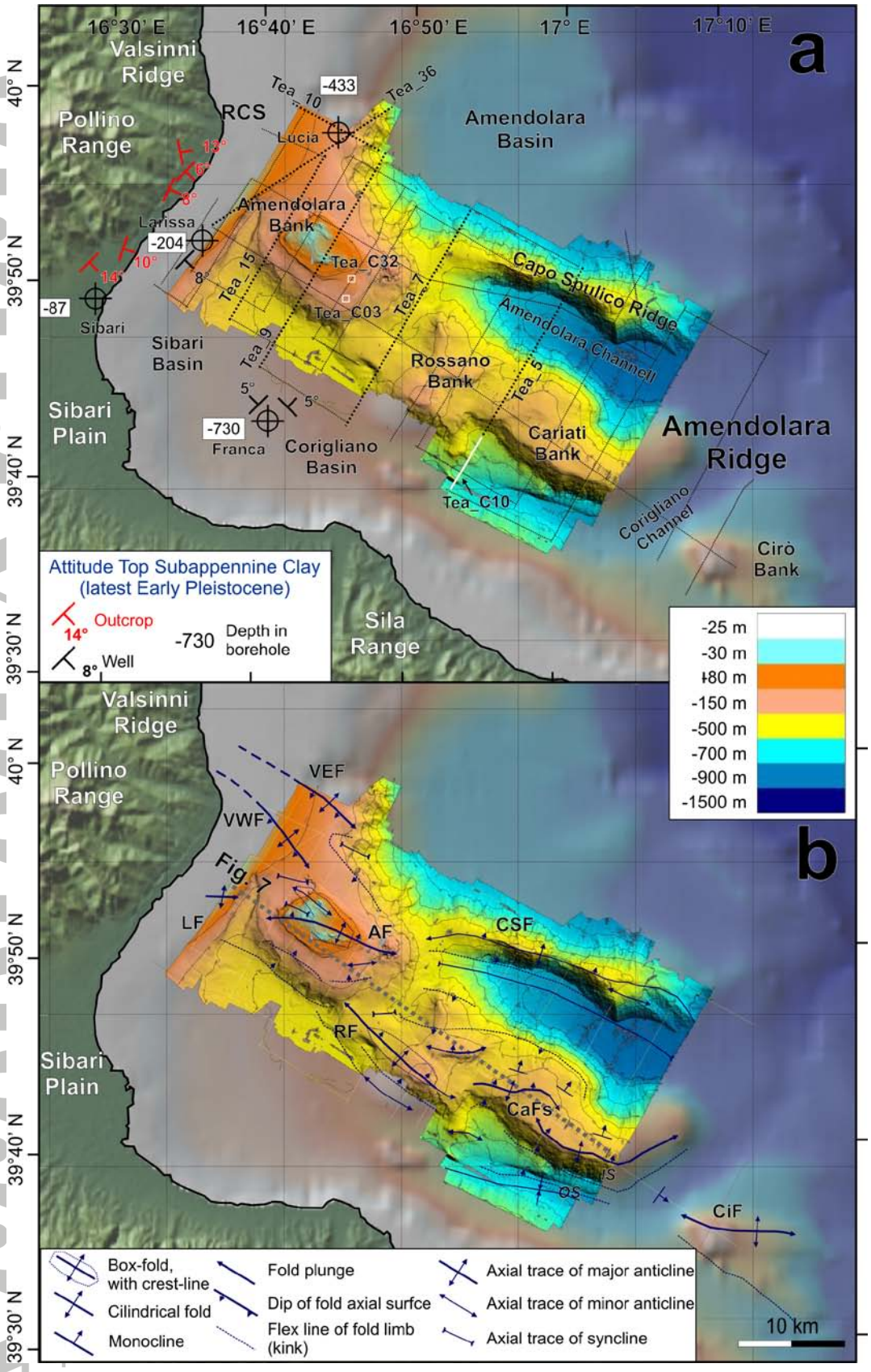

Figure 3. a) Morphobathymetric map of the Amendolara Ridge derived from the Teatioca_2011 multibeam survey, integrated with bathymetry data from GEBCO08 Digital

Atlas (www.nbi.ac.uk), showing the grid of acquired Sparker profiles (dotted black lines; thicker lines are selected profiles shown in Figure 4) and selected CHIRP profiles (white line and boxes). Attitude of the top of the Subapennine Clay in outcrop and in borehole (including depth) is also shown. Arrows attached to wells indicate line projection. RCS, Roseto Capo Spulico; b) Morpho-structural map of the Amendolara Ridge derived from interpretation of the Sparker profiles. Folds: AF, Amendolara Fold; CaFs, Cariati Folds; CiF, Cirò Fold; CSF, Capo Spulico Fold; LF, Larissa Fold; RF, Rossano Fold; VEF, Valsinni Eastern Fold; VWF, Valsinni Western Fold. IS and OS, Outer and Inner Scarp of the Cariati Bank, respectively.

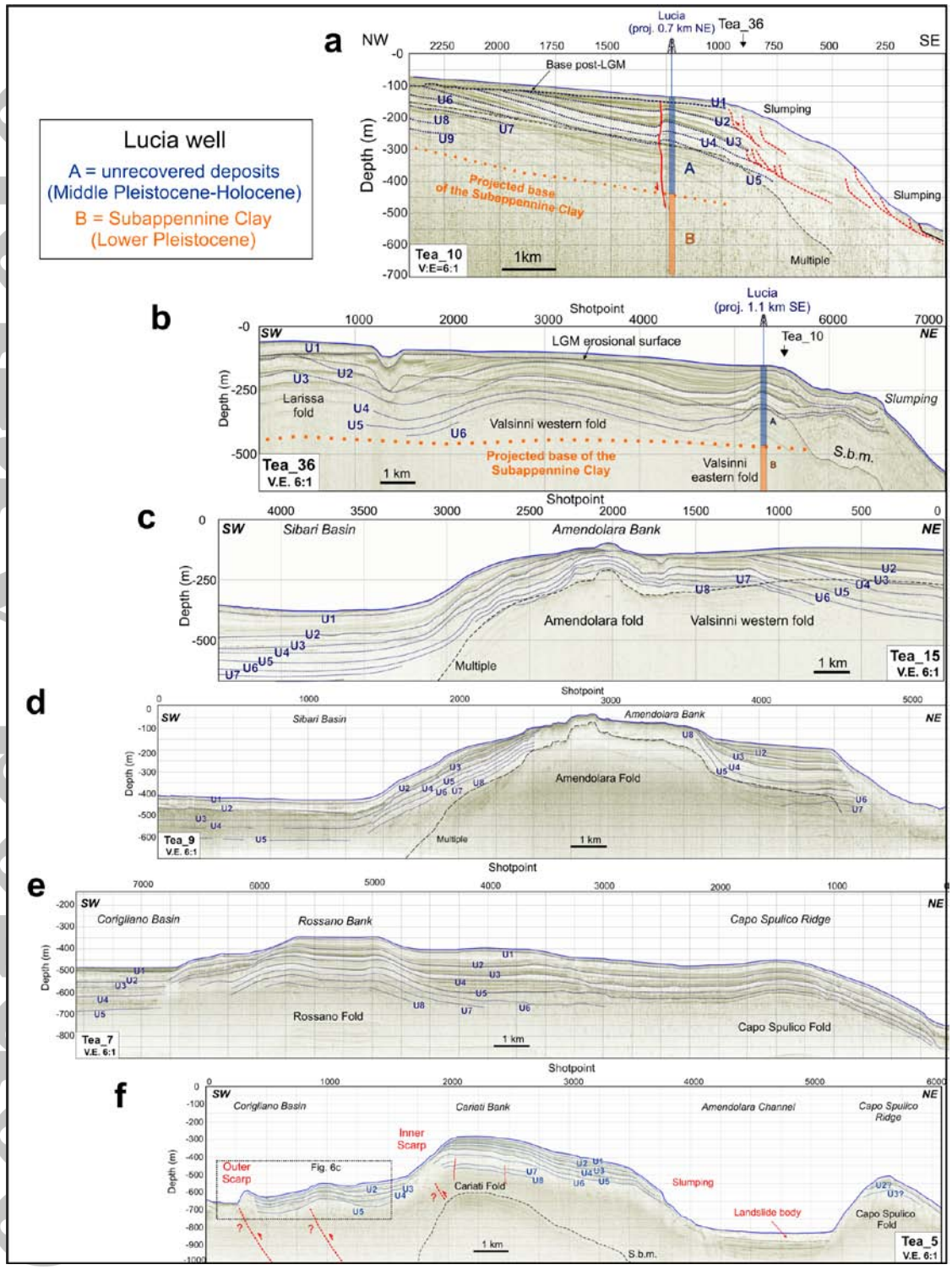

Figure 4. Depth-converted interpreted SCS lines through: a) and b) the Calabria shelf (Tea_10, Tea_36); c) and d) the Amendolara Bank (Tea_15, Tea_9); e) the Rossano Bank (Tea_7); f) the Cariati Bank (Tea_5), showing the identified seismic units and bounding basal unconformities (U). The upper section of borehole Lucia is displayed in profiles a) and b). The projected base of the top of the Subapennine Clay in profile a) is derived from

interpolation of outcrop and well attitude and well depth data shown in Figure 3a. Section traces located in Figure 3a. Vertical exaggeration (V.E.) = 6:1 for all profiles. Scale is the same for all profiles except for profile Tea_10 (a) where it is 1.5 times larger to better show the architecture and internal geometries of the sedimentary units. S. b. m., Sea-bottom multiple.

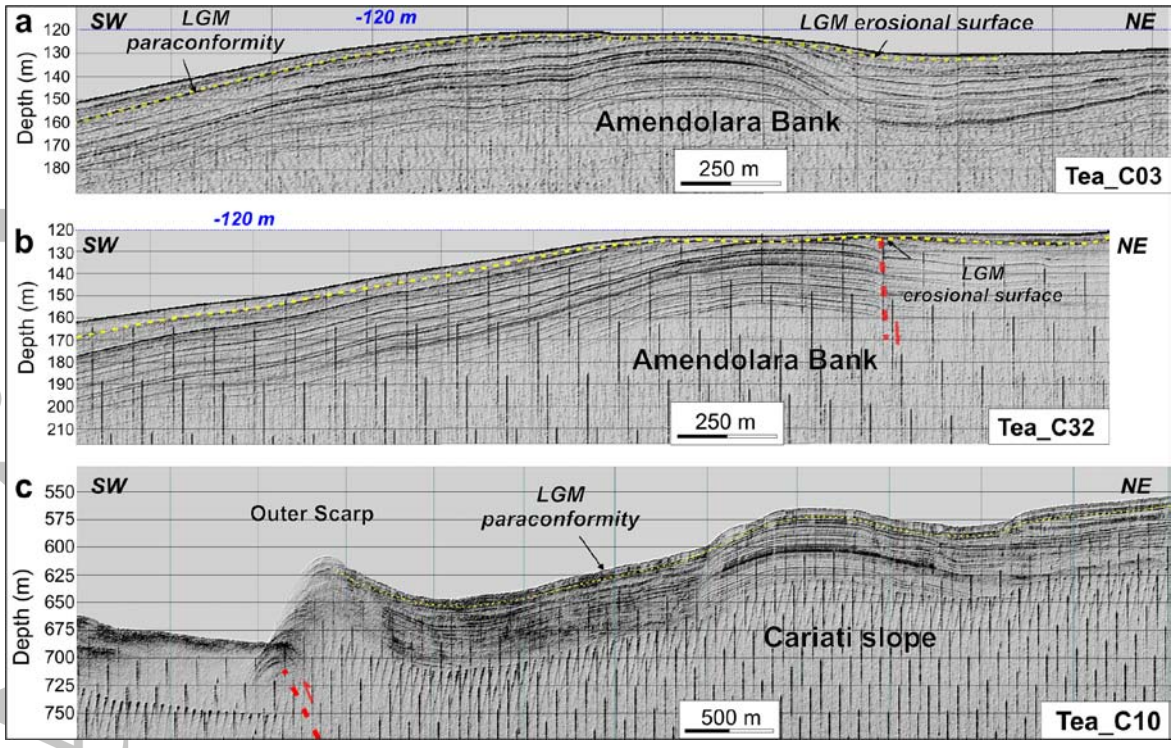

Figure 5. Depth-converted interpreted CHIRP lines through a) and b) the Amendolara Bank, and c) the southern slop of the Cariati Bank. Location in Fig. 3a.

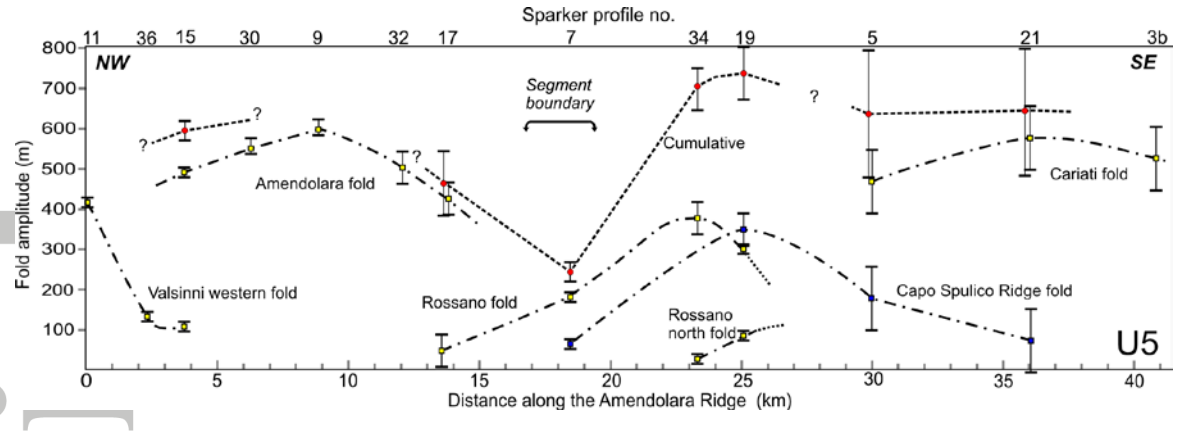

Figure 6. Pattern of fold amplitude measured for horizon U5 between anticline and syncline hinges on individual Sparker profiles (profile number indicated on top) along an idealized profile parallel to the Amendolara Ridge (generalized location in Figure 3b). On top of the Amendolara Bank, where U5 was eroded, the amplitude was assumed to coincide with the sea-floor. The amplitude pattern allows to distinguish different folds (dashed-dotted lines). The cumulative profile (dotted) is the sum of amplitude profiles for individual folds. The sharp amplitude decrease in the cumulative profile, as well as the termination of individual folds in the central part of the profile, identifies a segment boundary (arrow). A nominal uncertainty of ±10 m has been adopted when horizon picking was straightforward. Uncertainty is increased and asymmetric (-10/+20 m) in the case of erosional removal of the horizon on the Amendolara Bank. When correlation ambiguity was suspected, uncertainty has been increased to ±40 m, which takes into account a maximum error in horizon correlation to one sequence boundary above and below U5. Uncertainty has been further increased to ±80 m for the Cariati fold due to the lower resolution in greater water depths. Note that the fold amplitude estimation is a maximum bound because it assumes flat bathymetry prior to U5 development.

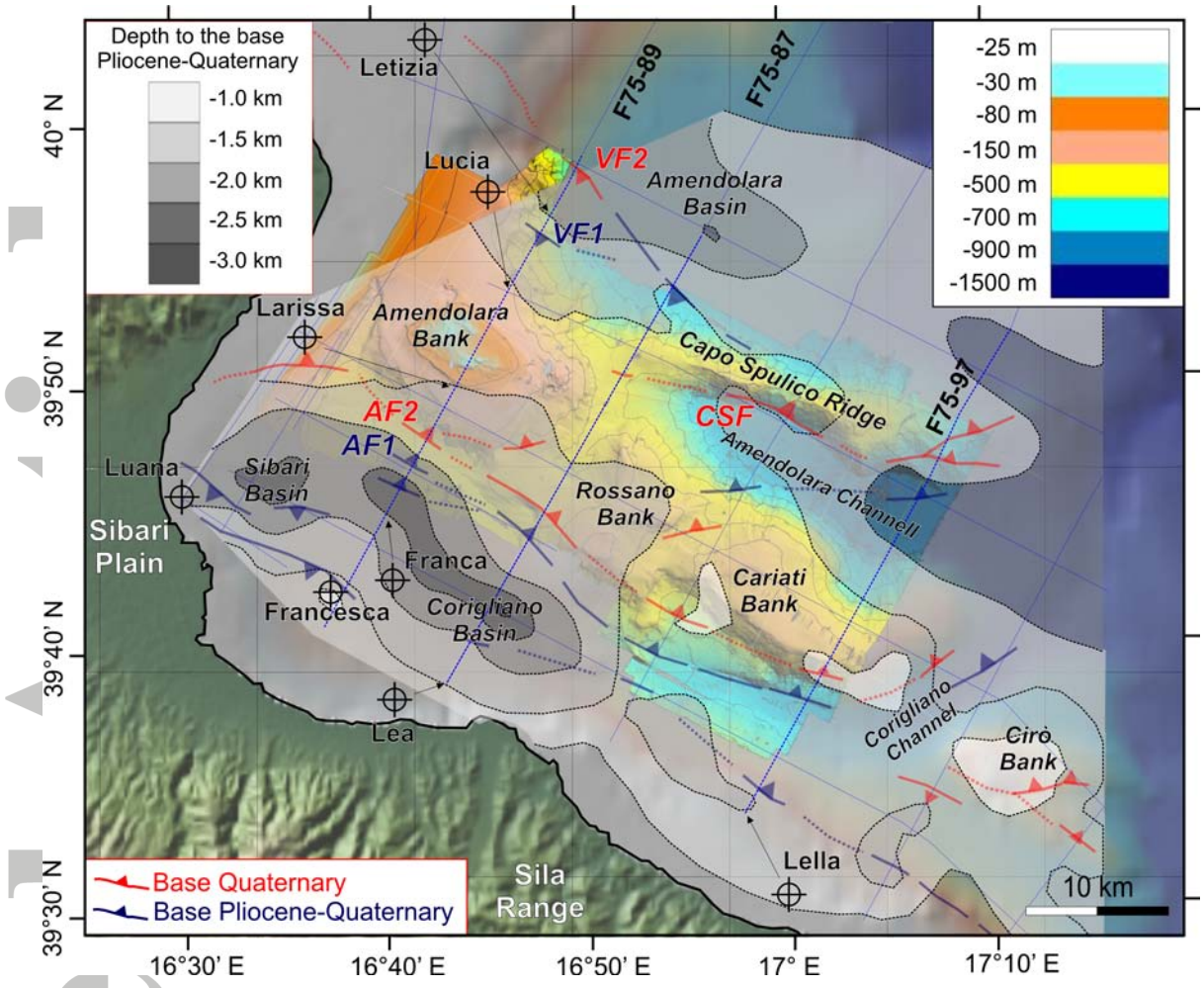

Figure 7. Structural map of the Amendolara Ridge derived from interpretation of the MCS profiles, showing age of last detectable fault activity, and the isobaths to the base of the Pliocene-Quaternary. The grid of profiles and the wells used to build the isobaths map are indicated. Arrows attached to wells indicate line projection. Highlighted and labeled profiles are shown in Figure 11. Individual faults strands of the Amendolara and Valsinni faults systems are labeled as AF1, Af2, and VF1, VF2, respectively. SB, Sibari Basin; CB, Corigliano Basin.

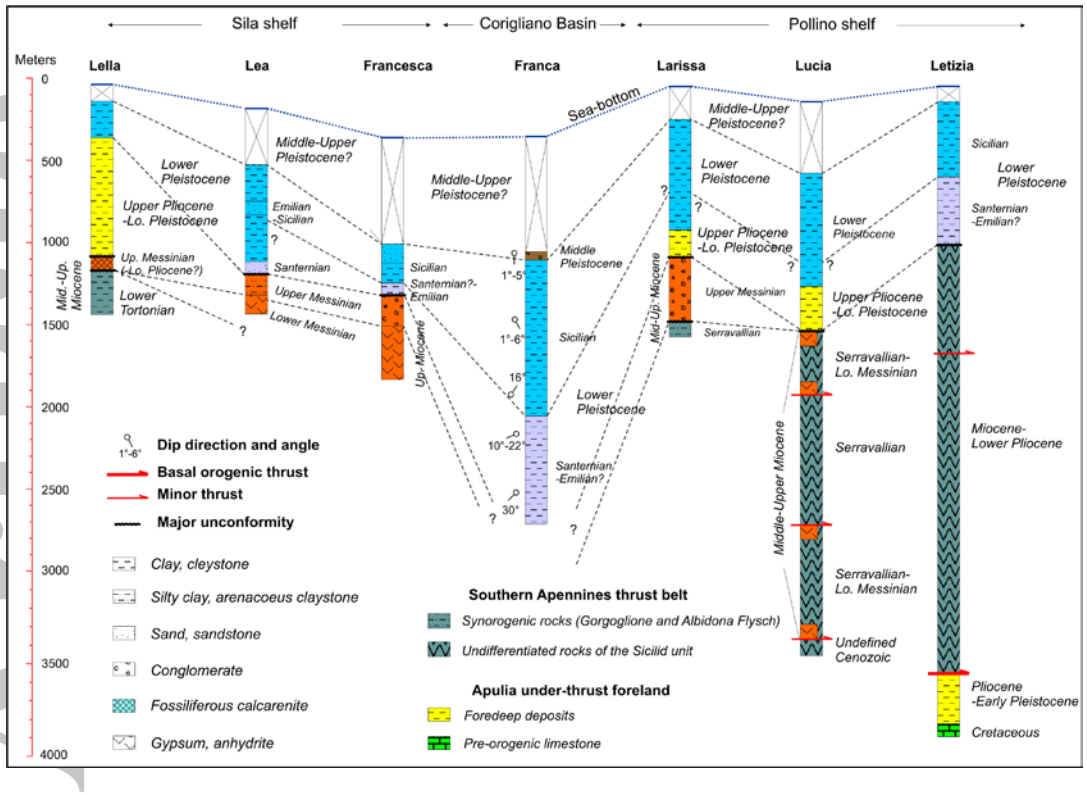

Figure 8. Stratigraphic correlation among 7 selected wells from the Sila to the Pollino shelf. Wells are located in Figure 8. Up., Upper. Lo., Lower.

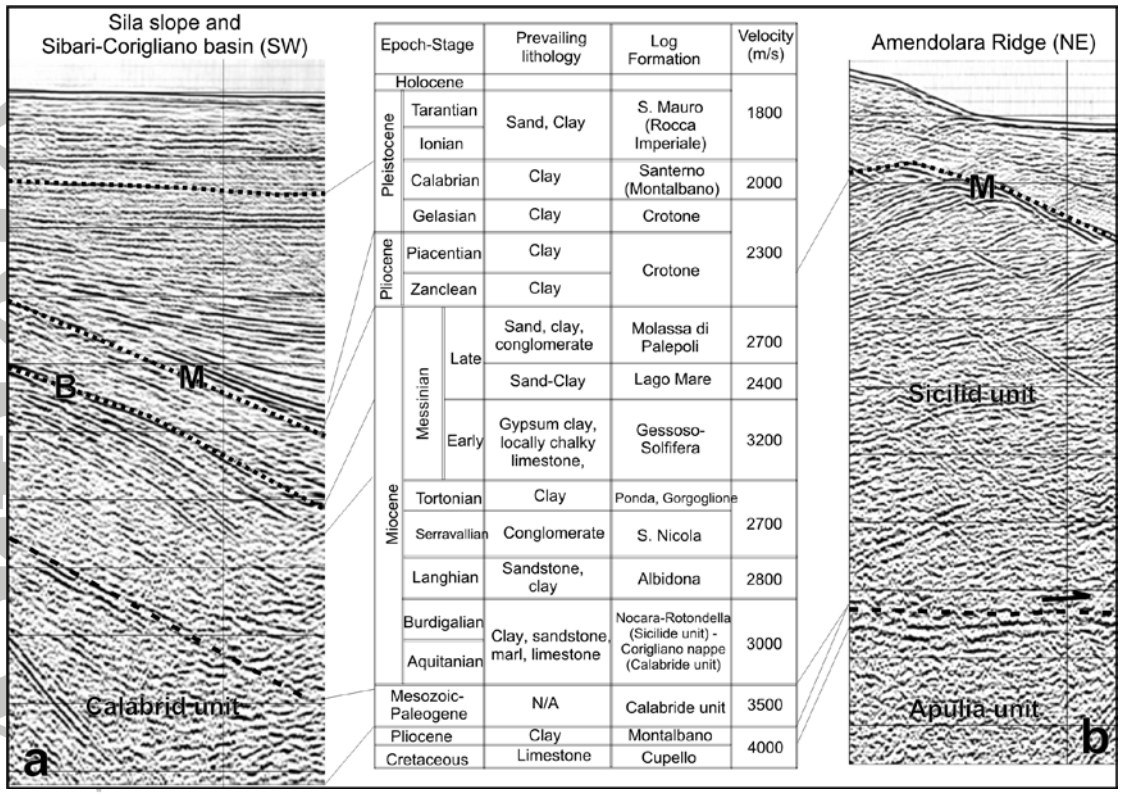

Figure 9. Seismostratigraphic frame of the sedimentary section in the Ionian offshore aligned along a general SW-NE cross section from the northern Sila shelf (a) to the Amendolara Ridge (b). Note that we did not trace reflector B on the seismic section in the right panel because it has been disrupted and duplicated by thrusting (see Lucia well, Fig, 8).

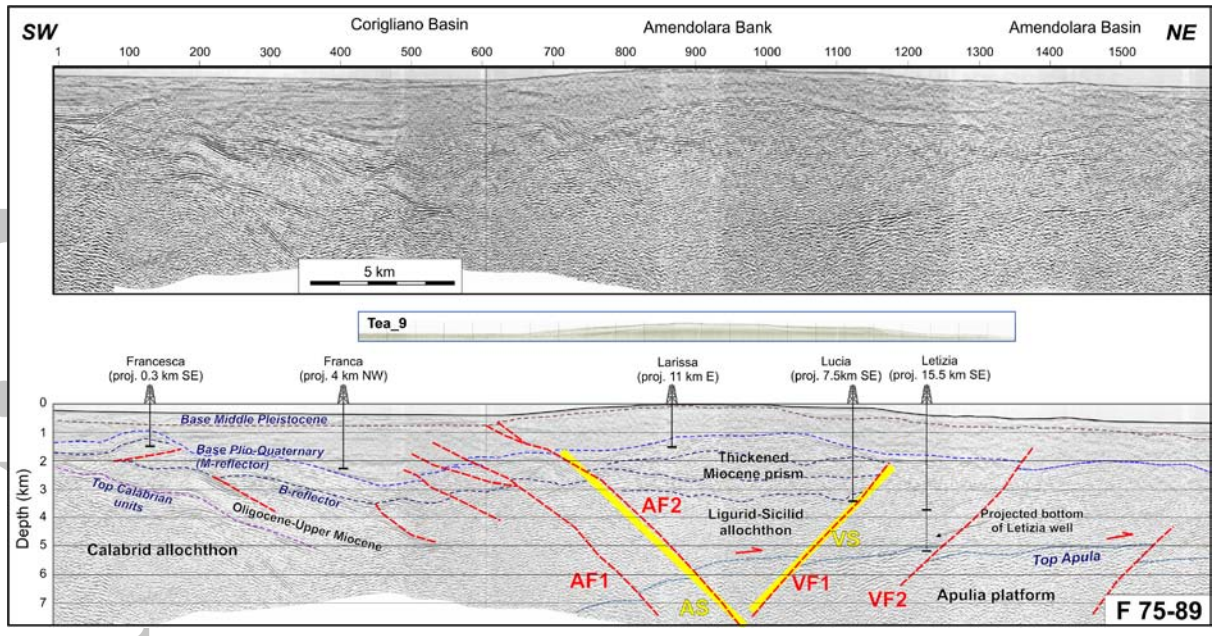

Figure 10a. (top) Time to Depth converted MCS seismic reflection profiles F75-89 (location in Figure 8). (bottom) Interpretation (modified after *Ferranti et al.* [2009]; *Santoro et al.* [2013]). Projection of oil explorations wells (located in Fig. 7) is reported. Note that the Letizia well is projected from a long distance and thus the bottom unit (Apulia) drilled by the well is located at a higher depth in the study area due to the structural slope. Because of this, the actual depth of the well has been projected further down-section till the Apulia unit. Faults labeled as in Figure 8. Thick yellow lines are faults segments from dislocation modeling. Inset shows the Sparker profile Tea_9 (no vertical exaggeration) whose trace coincides with that of the MCS line.

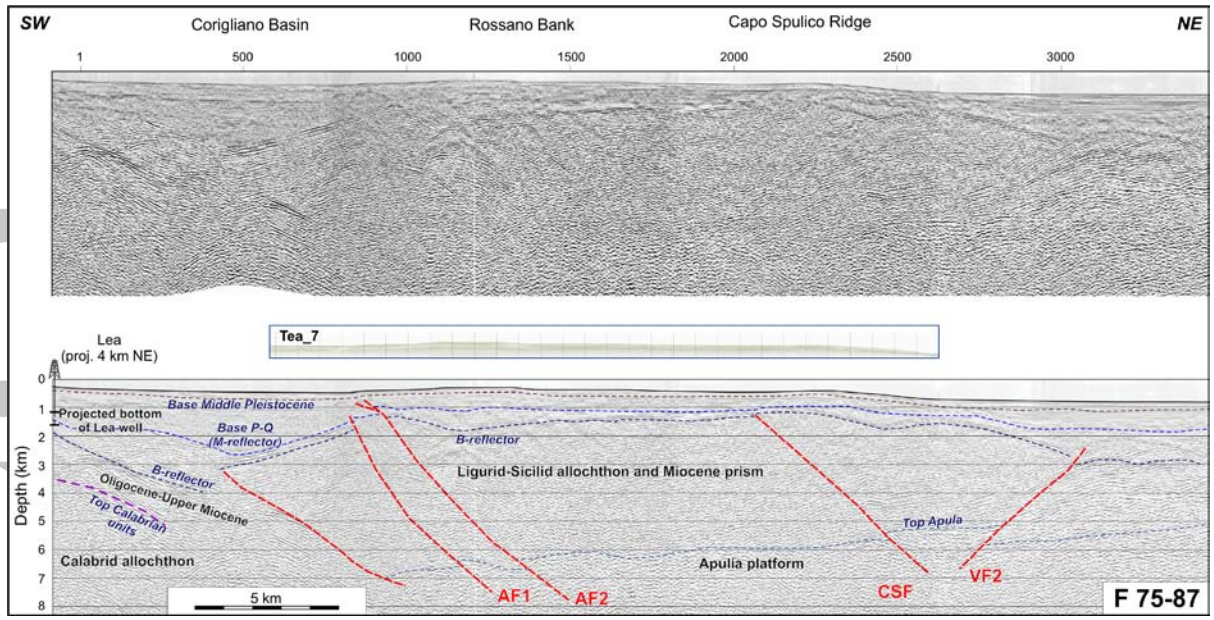

Figure 10b. (top) Time to Depth converted MCS seismic reflection profiles F75-87 (location in Figure 8). (bottom) Interpretation. Faults labeled as in Figure 8. Projection of the Lea oil explorations well (located in Fig. 7) along the section is reported. For the well depth-projection, see caption of Figure 10a. Inset shows the Sparker profile Tea_7 (no vertical exaggeration) whose trace coincides with that of the MCS line.

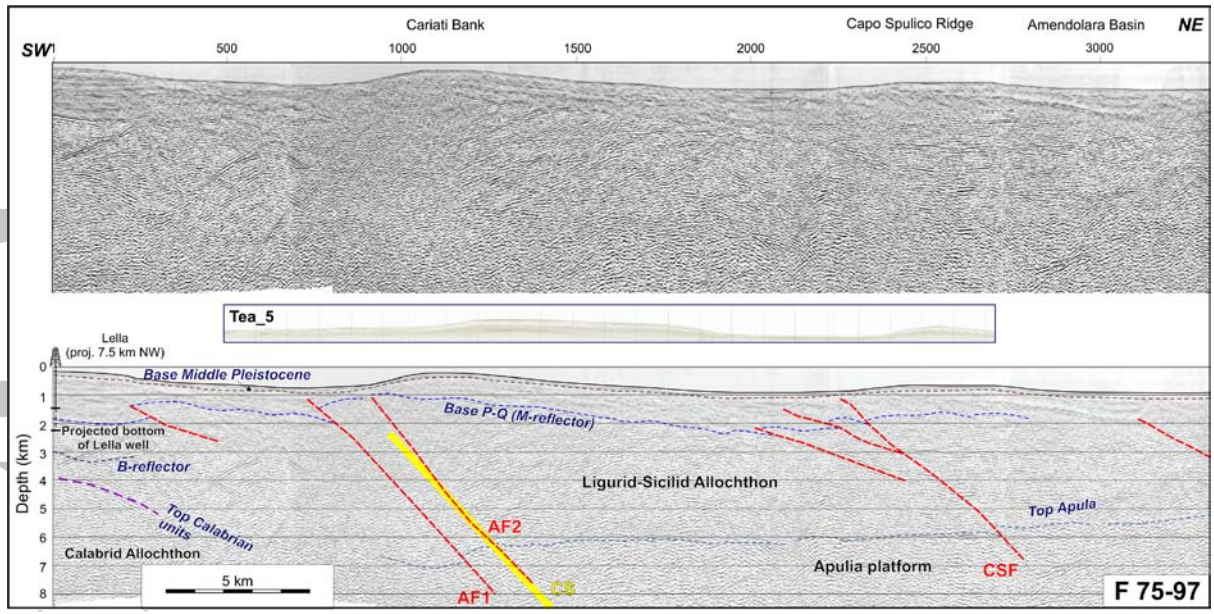

Figure 10c. (top) Time to Depth converted MCS seismic reflection profiles F75-97 (location in Figure 8). (bottom) Interpretation. Faults labeled as in Figure 8. Projection of the Lella oil explorations well (located in Fig. 7) along the section is reported. For the well depth-projection, see caption of Figure 10a. Thick yellow lines are faults segments from dislocation modeling. Inset shows the Sparker profile Tea_5 (no vertical exaggeration) whose trace parallels but does not coincides with that of the MCS line.

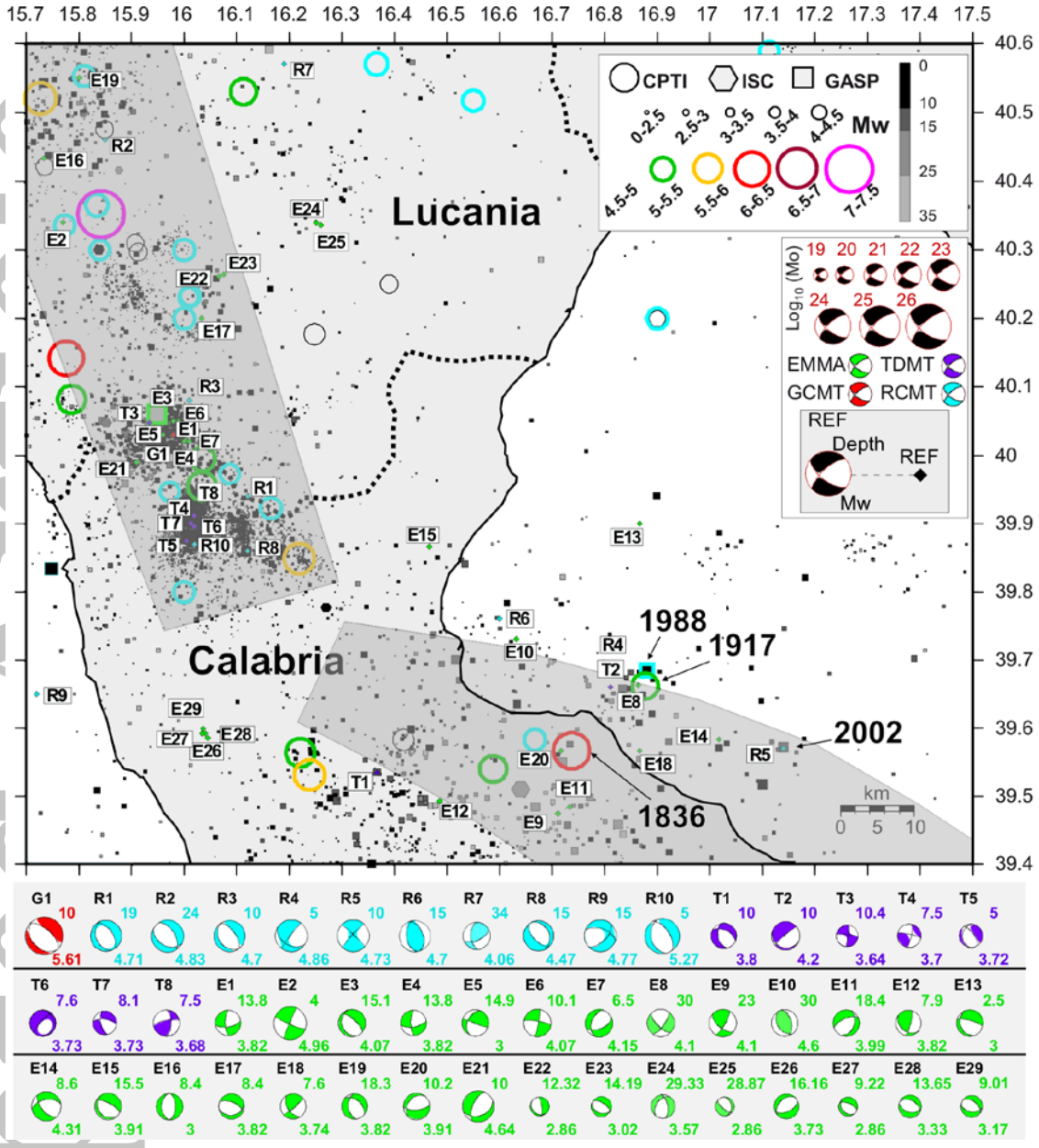

Figure 11. Seismicity data in Southern Lucania and Northern Calabria from various seismic catalogues (see text for detail). Symbols of the Parametric Catalog of Italian Earthquakes (CPTI11, Rovida et al. [2011]) are unfilled, without depth information. Depth, Mw and reference (see table S1) for each focal solution is displayed. Location of focal mechanisms in the map is indicated by colored diamonds with reference number. The dotted line outlines the regional administrative boundaries. The grey boxes include the two different seismic domains identified by Totaro et al. [2013]. For parameters details of the focal mechanisms see table S1.

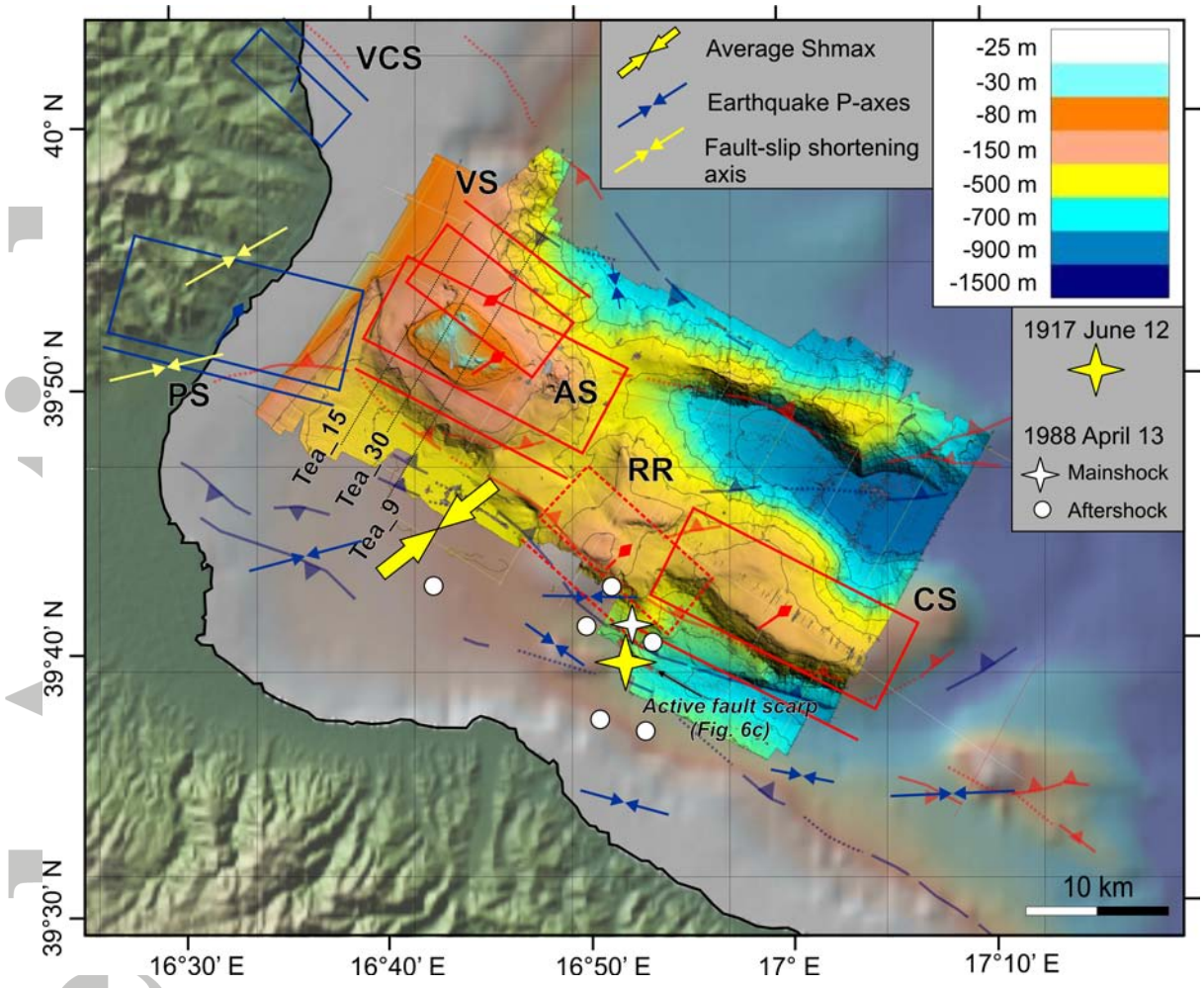

Figure 12. Seismotectonic map of the Amendolara Ridge showing thrust segments used in the dislocation modeling (solid boxes: segment; dashed box: relay ramp; red from this study, navy from *Santoro et al.* [2009]), epicenters of historical events (1917 event, and 1988 earthquake mainshock and aftershocks), and the trend of strain axis (average seismological Shmax axis from *Presti et al* [2013]; individual seismological P-axis from Figure 11 and Table S1; shortening axis derived from fault-slip inversion from *Ferranti et al.* [2009]). The Sparker lines used for elastic modeling (Figure S2) are indicated. Location of the active fault scarp detected from SCS profiles is shown. AS, Amendolara Segment; CS, Cariati Segment; RR, Rossano Relay; VS, Valsinni Segment; PS, Pollino Segment; VCS, Valsinni Coastal Segment. The parameters of the thrust segments are listed in Table 2.